Noninnocence of the Ligand Glyoxal-bis(2-mercaptoanil). The Electronic Structures of [Fe(gma)]₂, [Fe(gma)(py)]·py, [Fe(gma)(CN)]$^{1-/0}$, [Fe(gma)I], and [Fe(gma)(PR₃)$_n$] (n = 1, 2). Experimental and Theoretical Evidence for "Excited State" Coordination

Prasanta Ghosh, Eckhard Bill, Thomas Weyhermüller, Frank Neese,* and Karl Wieghardt*

Contribution from the Max-Planck-Institut für Strahlenchemie, Stiftstrasse 34-36, D-45470 Mülheim an der Ruhr, Germany

Received August 26, 2002 ; E-mail: wieghardt@mpi-muelheim.mpg.de; neese@mpi-muelheim.mpg.de

Abstract: The electronic structure of the known iron complexes [Fe(gma)]₂ (S_t = 0) (**1**)[6] and [Fe(gma)-(py)]·py (S_t = 1) (**2**)[7] where H₂(gma) represents glyoxal-bis(2-mercaptoanil) has been shown by X-ray crystallography, Mössbauer spectroscopy, and density functional theory calculations to be best described as ferric (S_{Fe} = 3/2) complexes containing a coordinated open-shell π radical trianion (gma•)$^{3-}$ and not as previously reported[6,7] as ferrous species with a coordinated closed-shell dianion (gma)$^{2-}$. Compound **1** (or **2**) can be oxidized by I₂ yielding [Fe^{III}(gma)I] (S_t = 1/2) (**3**). With cyanide anions, complex **1** forms the adduct [(n-Bu)₄N][Fe^{III}(gma•)(CN)] (S_t = 1) (**4**), which can be one-electron oxidized with iodine yielding the neutral species [Fe^{III}(gma)(CN)] (S_t = 1/2) (**5**). With phosphines complex **1** also forms adducts[7] of which [Fe^{III}(gma•)(P(n-propyl)₃)] (S_t = 1) (**6**) has been isolated and characterized by X-ray crystallography. [Fe^{II}-(gma)(P(n-propyl)₃)₂] (S_t = 0) (**7**) represents the only genuine ferrous species of the series. Density functional theory (DFT) calculations at the BP86 and B3LYP levels were applied to calculate the structural as well as the EPR and Mössbauer spectroscopic parameters of the title compounds as well as of the known complexes [Zn(gma)]$^{0/-}$ and [Ni(gma)]$^{0/-}$. Overall, the calculations give excellent agreement with the available spectroscopic information, thus lending support to the following electronic structure descriptions: The gma ligand features an unusually low lying LUMO, which readily accepts an electron to give (gma•)$^{3-}$. The one-electron reduction of [Zn(gma)] and [Ni(gma)] is strictly ligand centered and differences in the physical properties of [Zn(gma•)]$^-$ and [Ni(gma•)]$^-$ are readily accounted for in terms of a model that features enhanced back-bonding from the metal to the gma LUMO in the case of [Ni(gma•)]$^-$. In the case of [Fe(gma)(PH₃)], [Fe(gma)(py)], and [Fe(gma)(CN)]$^-$ an electron transfer from the iron to the gma LUMO takes place to give strong antiferromagnetic coupling between an intermediate spin Fe(III) (S_{Fe} = 3/2) and (gma•)$^{3-}$ (S_{gma} = 1/2), yielding a total spin S_t = 1. Broken symmetry DFT calculations take properly account of this experimentally calibrated electronic structure description. By contrast, the complexes [Fe(gma)(PH₃)₂] and [Fe(PhBMA)] feature closed-shell ligands with a low-spin Fe(II) (S_{Fe} = S_t = 0) and an intermediate spin central Fe(II) (S_{Fe} = S_t = 1), respectively. The most interesting case is provided by the one-electron oxidized species [Fe(gma)(py)]$^+$, [Fe(gma)I], and [Fe(gma)(CN)]. Here the combination of theory and experiment suggests the coupling of an intermediate spin Fe(III) (S_{Fe} = 3/2) to the dianionic ligand (gma)$^{2-}$ formally in its first excited triplet state (S_{gma} = 1) to give a resulting S_t = 1/2. All physical properties are in accord with this interpretation. It is suggested that this unique "excited state" coordination is energetically driven by the strong antiferromagnetic exchange interaction between the metal and the ligand, which cannot occur for the closed-shell form of the ligand.

Introduction

The coordination chemistry of the dianion of glyoxal-bis(2-mercaptoanil), H₂(gma) (Scheme 1), with transition-metal ions such as nickel(II), zinc(II), cadmium(II), or iron(II) has been investigated in some detail in the past.[1−6] The neutral species [M(gma)] (M = Zn,[1,3,4] Cd,[1,3] Ni,[2] and Fe[5]) have been isolated. Sellmann et al.[6] reported the crystal structure of dinuclear [Fe-

(gma)]₂ in 1992, which was the first crystallographically characterized complex containing a tetradentate (gma) ligand (Figure 1).

In these cases the oxidation state of the central metal ion has been assigned as divalent, +II, because the dianionic ligand (gma)$^{2-}$ was considered to possess a closed-shell electronic structure and zinc(II) and cadmium(II) (d^{10}) are also closed-shell systems giving rise to diamagnetic complexes [M^{II}(gma)]. The argument for diamagnetic, square-planar [Ni^{II}(gma)] is

(1) Jadamus, H.; Fernando, Q.; Freiser, H. *Inorg. Chem.* **1964**, *3*, 928.

Scheme 1. Ligands and Complexes
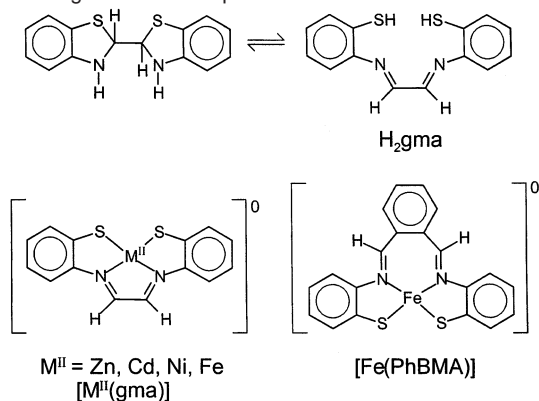
Complexes:

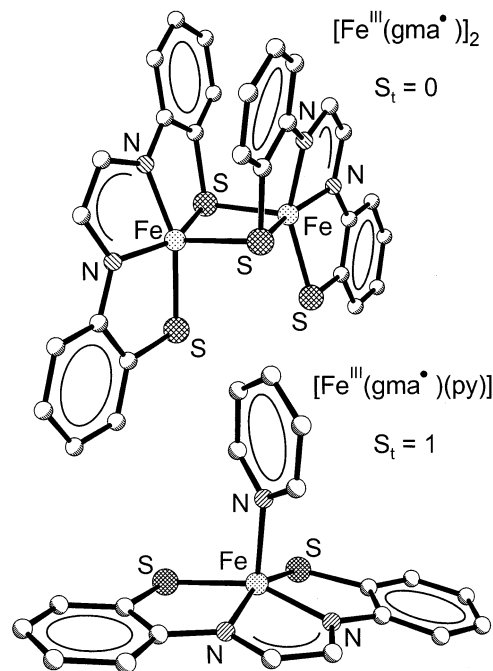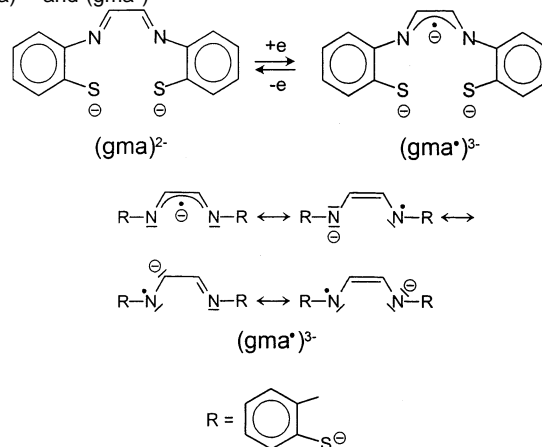|		
[Fe(gma)]$_2$	**1**	(ref. 5,6,7)
[Fe(gma)(py)]py	**2**	(ref. 7)
[Fe(gma)I]	**3**	
[(n-Bu)$_4$N]$_2$[Fe(gma)(CN)]	**4**	
[Fe(gma)(CN)]	**5**	
[Fe(gma)(P(n-propyl)$_3$)]	**6**	
[Fe(gma)(P(n-propyl)$_3$)$_2$]	**7**	
[Fe(Ph-BMA)]	**8**	(ref. 7)

Figure 1. Schematic view of the dimeric molecule (top) in crystals of **1** adapted from ref 6 and of the mononuclear neutral species (bottom) in crystals of **2** adapted from ref 7. The C−C, C−N, and C−S bond distances are listed in Table 2.

Scheme 2. Resonance Structures of the Dianion and Trianion (gma)$^{2-}$ and (gma•)$^{3-}$

similar.[2] The central nickel(II) ion has a d^8 electron configuration, giving rise to the observed $S = 0$ ground state in a square-planar ligand field.

Gray et al.[2] and Holm et al.[2] have also prepared and studied the paramagnetic monoanionic species [Ni(gma)]$^-$ ($S = 1/2$), the EPR spectrum of which has been measured ($g_1 = 1.979$, $g_2 = 2.006$, $g_3 = 2.028$ in 2-methyltetrahydrofuran). A definitive description of its electronic structure has not been given, although Gray et al.[2e] have noted that "it is very possible that the unpaired electron in [Ni(gma)]$^-$ actually resides in an orbital primarily delocalized over the α-diimine linkage." Holm et al. on the other hand pointed out that this description may be an oversimplified view.[2d] We show here that the monoanion can indeed be described as [Ni^{II}(gma•)]$^-$, where (gma•)$^{3-}$ is an open-shell, trianionic π radical (Scheme 2).

Busch et al.[5] in 1968, Sellmann et al.[6] in 1992, and Strähle et al.[7] in 1997 have all assigned the oxidation state of the central iron ion in the dinuclear species [Fe(gma)]$_2$ as +II (low spin d^6). It was felt[7] that the crystal structure and the Mössbauer spectral parameters (isomer shift 0.24 mm s^{-1} and quadrupole splitting 2.03 mm s^{-1} at 80 K) were in accord with this interpretation.

Interestingly, the reaction of [Fe(gma)]$_2$ (**1**) with pyridine yields, under anaerobic conditions, mononuclear [Fe(gma)(py)]•py (**2**), which is *paramagnetic*, $S_t = 1$.[7] This complex has also been structurally characterized and is shown in Figure 1. It is

unexpected and surprising that the geometrical details of the Fe(gma) units in the diamagnetic dinuclear and the paramagnetic mononuclear complex are within experimental error identical (Table 2)—despite seemingly differing local spin states at the iron ions in both species.

Even more surprising is the observation that the isomer shift of 0.27 mm s^{-1} and the quadrupole splitting of 2.33 mm s^{-1} of [Fe(gma)(py)] (**2**) is very similar to the parameters reported by the same group for dinuclear [Fe(gma)]$_2$ (**1**).[7]

It is difficult to rationalize the presumption that the ligand field of the square-based pyramidal FeN$_2$S$_3$ polyhedron in (**1**) is strong enough to enforce a low-spin configuration at the

(2) (a) Stiefel, E. I.; Waters, J. H.; Billig, E.; Gray, H. B. *J. Am. Chem. Soc.* **1965**, *87*, 3016. (b) Lalor, F.; Hawthorne, M. F.; Maki, A. H.; Darlington, K.; Davison, A.; Gray, H. B.; Dori, Z.; Stiefel, E. I. *J. Am. Chem. Soc.* **1967**, *89*, 2278. (c) Holm, R. H.; Balch, A. L.; Davison, A.; Maki, A. H.; Berry, T. E. *J. Am. Chem. Soc.* **1967**, *89*, 2866. (d) Maki, A. H.; Berry, T. E.; Davison, A.; Holm, R. H.; Balch, A. L. *J. Am. Chem. Soc.* **1966**, *88*, 1080. (e) Dori, Z.; Eisenberg, R.; Stiefel, E. I.; Gray, H. B. *J. Am. Chem. Soc.* **1970**, *92*, 1506.
(3) Bayer, E.; Breitmaier, E. *Chem. Ber.* **1968**, *101*, 1579.
(4) Corbin, J. L.; Work, D. E. *Can. J. Chem.* **1974**, *52*, 1054.

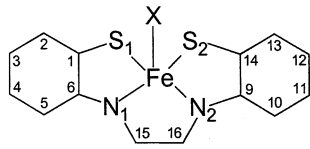(5) Elder, M. S.; Prinz, G. M.; Thornton, P.; Busch, D. H. *Inorg. Chem.* **1968**, *7*, 2426.
(6) Sellmann, D.; Hannakam, M.; Knoch, F.; Moll, M. *Z. Naturforsch.* **1992**, *47b*, 1545.
(7) Karsten, P.; Maichle-Mössner, C.; Strähle, J. *Z. Anorg. Allg. Chem.* **1997**, *623*, 1644.

Table 1. Crystallographic Data for **6**[a]

formula	$C_{23}H_{31}FeN_2PS_2$
crystal size, mm^3	$0.38 \times 0.10 \times 0.06$
fw	486.44
space group	$P2_12_12_1$, No. 19
a, Å	8.3100(4)
b, Å	15.6828(8)
c, Å	18.0724(12)
V, Å	2355.3(2)
Z	4
T, K	100(2)
ρ_{calcd}, g cm^{-3}	1.372
diffractometer used	Nonius Kappa-CCD
reflctns collected/θ_{max}	43848/59.98
unique reflctns/$I > 2\sigma(I)$	6850/6334
no. of params/restraints	269/2
μ(Mo Kα), cm^{-1}	8.98
R1^a/goodness of fit^b	0.0547/1.215
wR2^c ($I > 2\sigma(I)$)	0.1041

^{a} $I > 2\sigma(I)$. R1 $= \Sigma||F_o| - |F_c||/\Sigma|F_o|$. ^{b} GooF $= [\Sigma[w(F_o^2 - F_c^2)^2]/(n - p)]^{1/2}$. ^{c} wR2 $= [\Sigma[w(F_o^2 - F_c^2)^2]/\Sigma[w(F_o^2)^2]]^{1/2}$, where $w = 1/\sigma^2(F_o^2) + (aP)^2 + bP$, $P = (F_o^2 + 2F_c^2)/3$.

Table 2. Bond Distances (Å) of the Fe(gma)X Unit in **1**, **2**, and **6**

	1	**2**^{a}	**6**
Fe−S1	2.213(3)	2.211(1)	2.200(2)
Fe−S2	2.232(3)	2.218(1)	2.198(2)
Fe−N1	1.884(6)	1.900(3)	1.879(4)
Fe−N2	1.898(6)	1.907(3)	1.886(5)
S1−C1	1.756(8)	1.754(5)	1.773(6)
S2−C14	1.765(8)	1.755(4)	1.756(6)
N1−C6	1.408(12)	1.408(5)	1.398(7)
N2−C9	1.393(10)	1.412(5)	1.420(7)
N1−C15	1.363(11)	1.336(5)	1.375(7)
N2−C16	1.352(12)	1.330(5)	1.345(7)
C15−C16	1.391(10)	1.382(6)	1.354(7)
C1−C2	1.397(14)	1.396(6)	1.378(8)
C2−C3	1.393(14)	1.388(6)	1.390(9)
C3−C4	1.365(14)	1.376(5)	1.392(10)
C4−C5	1.392(13)	1.383(6)	1.363(9)
C5−C6	1.398(12)	1.392(6)	1.399(8)
C1−C6	1.377(10)	1.404(5)	1.394(8)
C9−C10	1.402(10)	1.395(6)	1.386(9)
C10−C11	1.384(13)	1.395(6)	1.381(10)
C11−C12	1.382(11)	1.386(6)	1.364(11)
C12−C13	1.376(12)	1.380(6)	1.379(10)
C13−C14	1.363(14)	1.392(6)	1.409(8)
C14−C9	1.417(10)	1.407(6)	1.413(8)
Fe−X^b	2.323(3)	2.076(3)	2.318(1)

^{a} Values are given for one crystallographically independent molecule only. ^{b} X = S in **1**, N in **2**, and P in **6**.

central ferrous ion, whereas the ligand field of the similar FeN$_3$S$_2$ polyhedron in (**2**) is so different that it produces an intermediate spin configuration at the ferrous ion ($S_{Fe} = 1$). Note that there is no other example in the literature for a five-coordinate ferrous ion with a genuine $S_{Fe} = 1$ ground state. Thus, we felt that the above model for the electronic structure of both compounds is not adequate, since it does not explain the structural and spectroscopic features of these complexes in a consistent and satisfactory manner.

Therefore, we have synthesized a new series of complexes (Scheme 1) containing the Fe(gma) unit and studied their structural and electronic properties by X-ray crystallography,

EPR, UV−vis, and Mössbauer spectroscopy and magnetochemistry. In addition, we have used density functional theory in order to rationalize in a consistent fashion the experimental data by a bonding model for these complexes.

As we will conclusively show here, the ligand (gma) in these complexes is noninnocent in the sense that it can be coordinated as a closed-shell dianion, (gma)$^{2-}$, or as an open-shell π radical trianion, (gma$^{\bullet}$)$^{3-}$, and, as we also suggest here, as a dianion in an excited triplet state, (gma*)$^{2-}$. The resonance structures shown in Scheme 2 imply the following structural differences between the coordinated dianion (gma)$^{2-}$ and its reduced trianion (gma$^{\bullet}$)$^{3-}$: (i) the C−C bond distance of the ethylene bridge is longer in the dianion (C−C single bond) than in the trianion and (ii) the two C−N bond distances of the bridge are shorter in the dianion (C=N double bond) than in the trianion. The experimental studies are then combined with theoretical DFT calculations to arrive at an experimentally calibrated bonding scheme. It is emphasized that in order to correctly identify the complex electronic features of the molecules studied in this work, it is of critical importance to connect theory and experiment through the prediction of spectral parameters. Methods to accomplish this task have recently been developed[9−16] and will prove to be of major utility in the present study. Few of the conclusions drawn in this paper could have been obtained from energetic considerations alone, since most of the molecules studied here have several low-lying states, all within the most optimistic error bounds of present day DFT methods (2−3 kcal/mol).[17]

Experimental Section

The dinuclear species [Fe(gma)]$_2$ (**1**) and the mononuclear species [Fe(gma)(py)]·py (**2**) have been prepared as described in ref 7.

[Fe(gma)I] (3). To a slurry of **1** (0.10 g; 0.15 mmol) and 1 mL of pyridine was added CH$_2$Cl$_2$ (1 mL) under an argon atmosphere. The solution was stirred for 45 min at 20 °C and filtered. To the filtrate a solution of iodine (30 mg; 0.24 mmol) in CH$_2$Cl$_2$ (20 mL) was added dropwise with stirring. A black, microcrystalline solid precipitated, which was filtered off and dried in air. Yield: 0.65 g (48%). Anal. Calcd for C$_{14}$H$_{10}$N$_2$S$_2$IFe: C, 37.08; H, 2.20; N, 6.18; S, 14.13; I, 28.03; Fe, 12.36. Found: C, 37.0; H, 2.3; N, 6.1; S, 14.5; I, 28.2; Fe, 12.4.

[(n-Bu)$_4$N][Fe(gma)(CN)]·1.5CH$_2$Cl$_2$ (4·1.5CH$_2$Cl$_2$). To a suspension of **1** (0.165 g; 0.25 mmol) in CH$_2$Cl$_2$ (40 mL) was added dropwise a solution of [(n-Bu)$_4$N]CN (0.135 g; 0.50 mmol) in CH$_2$Cl$_2$ (20 mL) under an Ar atmosphere with stirring. The resulting dark brown solution

(8) ShelXTL V.5, Siemens Analytical X-ray Instruments, Inc., 1994.
(9) Neese, F.; Solomon, E. I. *Inorg. Chem.* **1998**, *37*, 6568.
(10) (a) Neese, F.; *J. Chem. Phys.* **2001**, *115*, 11080 . (b) Neese, F. *Int. J. Quantum Chem.* **2001**, *83*, 104.
(11) F. Neese, *J. Phys. Chem. A* **2001**, *105*, 4290.
(12) Neese, F. *Inorg. Chim. Acta* **2002**, *337*, 181.
(13) (a) Munzarova, M. L.; Kaupp, M. *J. Phys. Chem. A* **1999**, *103*, 9966. (b) Munzarova, M. L.; Kubacek, P.; Kaupp, M. *J. Am. Chem. Soc.* **2000**, *122*, 11900.
(14) (a) Schreckenbach, G.; Ziegler, T. *J. Phys. Chem. A* **1997**, *101*, 3388. (b) Malkina, O. L.; Vaara, J.; Schimmelpfenning, B.; Munzarova, M.; Malkin, V.; Kaupp, M. *J. Am. Chem. Soc.* **2000**, *122*, 9206. (c) Kaupp, M.; Reviakine, R.; Malkina, O. L.; Arbuznikov, A.; Schimmelpfennig, B.; Malkin, V. *J. Comput. Chem.* **2001**, *23*, 794. (d) Patchkovskii, S.; Ziegler, T. *J. Phys. Chem. A.* **2001**, *105*, 5490.
(15) (a) Van Lenthe, E.; Wormer, P. E. S.; van der Avoird, A. *J. Chem. Phys.* **1997**, *107*, 2488. (b) Van Lenthe, E.; van der Avoird, A.; Wormer, P. E. S. *J. Chem. Phys.* **1998**, *108*, 4783.
(16) For review, see: (a) Neese, F.; Solomon, E. I. *Magnetoscience - From Molecules to Materials*; Miller, J. S., Drillon, M., Eds.; Wiley: New York, in press. (b) Kaupp, M. In: Lund, A., Shiotani, M., Eds. *EPR Spectroscopy of Free Radicals in Solids. Trends in Methods and Applications*; Kluwer: Dordrecht.
(17) Koch, W.; Holthausen, M. C. *A Chemist's guide to Density Functional Theory*; Wiley-VCH: Weinheim, 2000.

was filtered under argon and 20 mL of *n*-hexane were added. Upon slow evaporation of the solvent under reduced pressure a black microcrystalline precipitate formed, which was collected by filtration, washed with *n*-hexane, and dried. Yield: 0.21 g (70%). Anal. Calcd for $C_{31}H_{46}N_4S_2Fe \cdot 1.5CH_2Cl_2$: C, 54.06; H, 6.84; N, 7.76. Found: C, 54.2; H, 6.7; N, 7.9.

[Fe(gma)(CN)]·0.5CH₂Cl₂ (5·0.5CH₂Cl₂). To a suspension of **1** (0.20 g; 0.30 mmol) in CH_2Cl_2 (50 mL) was added dropwise with stirring under an argon atmosphere a solution of [(*n*-Bu)₄N]CN (0.165 g; 0.61 mmol) in CH_2Cl_2 (20 mL). To the resulting dark brown solution was added a solution of iodine (0.079 g; 0.62 mmol) in CH_2Cl_2 (20 mL) with stirring. A black solid precipitated which was collected by filtration, washed with CH_2Cl_2, and dried in air. Yield: 0.18 g (83%). Anal. Calcd for $C_{15}H_{10}N_3S_2Fe \cdot 0.5CH_2Cl_2$: C, 47.17; H, 2.81; N, 10.65; S, 16.24; Fe, 14.14. Found: C, 47.6; H, 3.2; N, 10.4; S, 15.9; Fe, 14.1.

[Fe(gma)(P(*n*-propyl)₃)] (6). To **1** (0.10 g; 0.15 mmol) was added tris(*n*-propyl)phosphine, P(*n*-propyl)₃, (0.055 g; 0.34 mmol), and CH_2Cl_2 (50 mL) under an argon atmosphere. After stirring for 45 min at 20 °C a dark brown solution, which was filtered, was obtained. Addition of *n*-heptane (20 mL) and evaporation of most of the solvent under reduced pressure produced a microcrystalline black solid. Yield: 0.08 g (55%). Anal. Calcd for $C_{23}H_{31}N_2S_2PFe$: C, 56.79; H, 6.42; N, 5.76. Found: C, 56.5; H, 6.5; N, 5.7.

Physical Measurements. Electronic spectra of the complexes in solution were recorded on a HP 8542A diode array spectrophotometer (range: 220−1200 nm). Temperature-dependent (2−298 K) magnetization data were recorded on a SQUID magnetometer (MPMS Quantum design) in an external magnetic field of 1.0 T. The experimental susceptibility data were corrected for underlying diamagnetism by the use of tabulated Pascal's constants. X-band EPR spectra were recorded on a Bruker ESP 300 spectrometer. The spectra were simulated by iteration of the anisotropic *g* values, hyperfine coupling constants, and line widths. Mössbauer data were recorded on an alternating constant-acceleration spectrometer. The minimum experimental line width was 0.24 mm s⁻¹ (full width at half-height). A constant sample temperature was maintained with an Oxford Instruments Variox or an Oxford Instruments Mössbauer-spectromag cryostat. The ⁵⁷Co/Rh source (1.8 GBq) was positioned at room-temperature inside the gap of the magnet system at a zero-field position. Reported isomer shifts (δ) are referenced vs iron metal at 300 K.

X-ray Crystallographic Data Collection and Refinement of the Structure. A dark brown single crystal of **6** was coated with perfluoropolyether, picked up with a glass fiber, and mounted in the nitrogen cold stream of the diffractometer. Intensity data were collected at 100(2) K by using graphite monochromated Mo Kα radiation (λ = 0.710 73 Å). Final cell constants were obtained from a least-squares fit of a subset of several thousand strong reflections. Data collection was performed by a full-sphere run taking frames at 0.9° in ω. A semiempirical absorption correction was tested but it did not improve the structure quality significantly. Intensity data were therefore left uncorrected for absorption effects. The ShelXTL software package[8] was used for solution, refinement, and artwork of the structure, which was readily solved by Patterson methods and difference Fourier techniques. All non-hydrogen atoms were refined anisotropically and hydrogen atoms were placed at calculated positions and refined as riding atoms with isotropic displacement parameters.

A propyl group of the P(pr)₃ ligand was found to be disordered. A satisfactory model was obtained by refining two split positions of carbon atoms C(21), C(22), and C(23). The occupancy factor of the two split groups was refined, keeping the corresponding C−C distances equal within a certain error and using the same anisotropic displacement parameters for each of the three split pairs. The absolute structure parameter could not be reliably determined, since the structure appeared to be racemically twinned. Crystallographic data and the diffractometer used are listed in Table 1; Table 2 summarizes bond distances of the Fe(gma) structural motif in complexes **1**, **2**, and **6**.

DFT Calculations. All calculations reported in this paper on complexes $[M(gma)(X)]^n$ (M = Zn, Ni, Fe; X = pyridine, CN⁻, PH₃, I⁻, Cl⁻; n = 0, ±1) were done with the program package ORCA.[18] Unless otherwise indicated, all geometry optimizations were carried out at the BP86 level[19,20] of DFT. This functional has proved in many applications its ability to reliably predict structures of transition metal complexes. The all-electron Gaussian basis sets used were those reported by the Ahlrichs group.[21] Accurate triple-ζ valence basis sets with one set of polarization functions on the metals, nitrogens, sulfurs, and axial ligands X were used (TZV(P)).[21b] The carbon and hydrogen atoms were described by a slightly smaller polarized split-valence SV(P) basis set that is of double-ζ quality in the valence region and contains a polarizing set of d-functions on the non-hydrogen atoms.[21a] The auxiliary basis sets used to fit the electron density were taken from the TurboMole library[22] and were chosen to match the orbital basis.

Unless otherwise indicated the SCF calculations were of the spin-polarized type and were tightly converged (10⁻⁷ Eh in energy, 10⁻⁶ Eh in the density change and 10⁻⁶ in maximum element of the DIIS[23] error vector). The geometry search was carried out in Cartesian displacement coordinates without imposing symmetry constraints but with translational and rotational degrees of freedom projected out. The geometries were considered converged after the energy change was less than 10⁻⁵ Eh, the gradient norm and maximum gradient element were smaller than 5 × 10⁻⁴ Eh/bohr and 10⁻³ Eh/Bohr, respectively, and the root-mean square and maximum displacements of atoms were smaller than 10⁻³ Bohr. Vibrational frequencies were calculated by numerical differentiation of analytical gradients and showed that all structures reported here are indeed minima on the potential energy surface.

Single point calculations with the B3LYP functional[19,24] were carried out at the optimized geometries in order to predict EPR[9,10,11] and Mössbauer[12] spectral parameters. For the quadrupole moment of ⁵⁷Fe the value 0.15 barn was used in place of the more common value of 0.2 barn.[25] This choice is based on the finding that the B3LYP DFT calculations tend to overestimate the quadrupole splitting and there is considerable uncertainty in the literature about the best choice of the quadrupole moment of the iron nucleus. In these calculations the same basis sets were used as in the geometry optimization, except for the metal basis which was the triply polarized "Core Properties" (CP(PPP)) basis described earlier.[12] Special care was taken in the numerical integration procedure to accurately integrate the electron density in the core region as is required for the prediction of Mössbauer isomer shifts.[12] In addition, the iron basis contained two polarizing p-functions with Wachters exponents[26] and one additional f-function from the TurboMole library with exponent 2.5.[22] For the analysis of the bonding in the complexes the canonical Kohn−Sham orbitals were localized according to the Pipek-Mezey criterion[27] and visualized through the interface of ORCA to the gOpenMol program.[28] Alternatively, broken symmetry (BS) type spin-unrestricted solutions were analyzed via the

(18) Neese, F. ORCA−an ab initio, DFT, and Semiempirical Electronic Structure Package. Version 2.2, Revision 14, Max-Planck Institut für Strahlenchemie, Mülheim, Germany, May 2002.
(19) Becke, A. D. *J. Chem. Phys.* **1988**, *84*, 4524.
(20) Perdew, J. P. *Phys. Rev. B* **1986**, *33*, 8822.
(21) (a) Schäfer, A.; Horn, H.; Ahlrichs, R. *J. Chem. Phys.* **1992**, *97*, 2571. (b) Schäfer, A.; Huber C.; Ahlrichs, R. *J. Chem. Phys.* **1994**, *100*, 5829.
(22) Basis sets were obtained from the ftp server of the quantum chemistry group at the university of Karlsruhe (Germany) under http://www.che-mie.uni-karlsruhe.de/PC/TheoChem/.
(23) (a) Pulay, P. *Chem. Phys. Lett.* **1980**, *73*, 393. (b) Pulay, P. *J. Comput. Chem.* **1992**, *3*, 556.
(24) (a) Lee, C.; Yang, W.; Parr, R. G. *Phys. Rev. B* **1988**, *37*, 785. (b) Becke, A. D. *J. Chem. Phys.* **1993**, *98*, 5648.
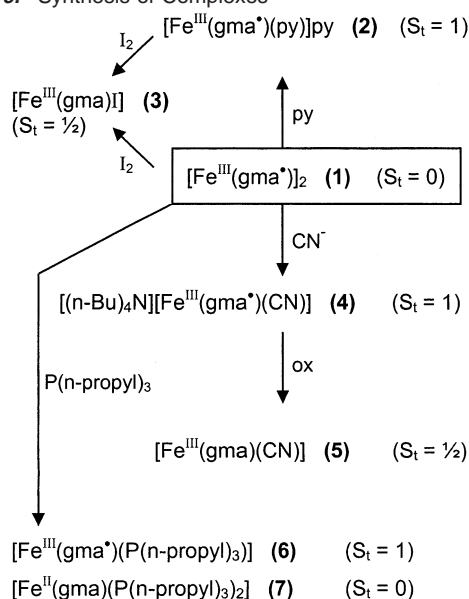(25) Dufek, P.; Blaha, P.; Schwarz, K. *Phys. Rev. Lett.* **1995**, *75*, 3545.
(26) (a) Wachter, A. J. H. *J. Chem. Phys.* **1970**, *52*, 1033. (b) Hay, P. J. *J. Chem. Phys.* **1977**, *66*, 4377.
(27) Pipek, J.; Mezey, P. G. *J. Chem. Phys.* **1989**, *90*, 4916.
(28) Laaksonen, L. The gOpenMol effort, Version 1.4, Espoo, Finland, 2000, obtained from http://www.csc.fi/~laaksone/gopenmol/gopenmol.html.

Scheme 3. Synthesis of Complexes

[Fe^{III}(gma$^\bullet$)(py)]py **(2)**   (S_t = 1)

I$_2$

[Fe^{III}(gma)I] **(3)**
(S_t = ½)

I$_2$

[Fe^{III}(gma$^\bullet$)]$_2$ **(1)**   (S_t = 0)

py

CN$^-$

[(n-Bu)$_4$N][Fe^{III}(gma$^\bullet$)(CN)] **(4)**   (S_t = 1)

ox

[Fe^{III}(gma)(CN)] **(5)**   (S_t = ½)

P(n-propyl)$_3$

[Fe^{III}(gma$^\bullet$)(P(n-propyl)$_3$)] **(6)**   (S_t = 1)
[Fe^{II}(gma)(P(n-propyl)$_3$)$_2$] **(7)**   (S_t = 0)

corresponding orbital transformation[29] and the spin-unrestricted natural orbitals. Note that in the latter two cases the orbitals do not have a well-defined orbital energy. In the figures showing such orbitals we therefore do not give orbital energies explicitly. It is the occupation and spin-coupling patterns that are our main interest in this case.

Results

Preparation of Complexes. Scheme 3 summarizes the complexes prepared. The reaction of the ligand H$_2$gma (or its derivative 2,2′-bisbenzthiazoline, shown in Scheme 1) with Fe^{II}-(acetate)$_2$ (1:1) in methanol under strictly anaerobic conditions yields solid [Fe(gma)]$_2$ (**1**) in 67% yield;[7] its crystal structure (Figure 1) has been reported[6] as well as its Mössbauer spectrum.[7] From susceptibility measurements, effective magnetic moments of 0.16 μ_B at 300 K and 0.09 μ_B per iron ion at 80 K have been reported.[7] Thus, **1** is diamagnetic with a singlet ground state. As stated above, based on these results all previous investigations have assigned a low-spin ferrous (d^6, S_{Fe} = 0) electron configuration to the iron ion and a closed-shell configuration for the ligand (gma)$^{2-}$.

Strähle et al.[7] and Sellmann et al.[6] have shown that **1** forms adducts with pyridine generating [Fe(gma)(py)]·py (**2**) (Figure 1), and with phosphines five- and six-coordinated complexes [Fe(gma)(PR$_3$)] and [Fe(gma)(PR$_3$)$_2$] have been isolated. Interestingly, both **2**[7] and [Fe(gma)(PR$_3$)][6] complexes are mononuclear paramagnetic species with an S_t = 1 ground state. For the latter this is shown here for the first time.[30] In contrast, the six-coordinate complexes *trans*-[Fe(gma)(PR$_3$)$_2$] are diamagnetic[6]—a surprising result. We have prepared the brown complex [Fe(gma)(P(*n*-propyl)$_3$)] (**6**) which converts to a violet six-coordinate species [Fe(gma)(P(*n*-propyl)$_3$)$_2$] (**7**) in solution with excess phosphine. Between 80 and 250 K a nearly temperature-independent magnetic moment of ~2.8 μ_B has been measured for solid **6** (S_t = 1); **7** is diamagnetic in solution.
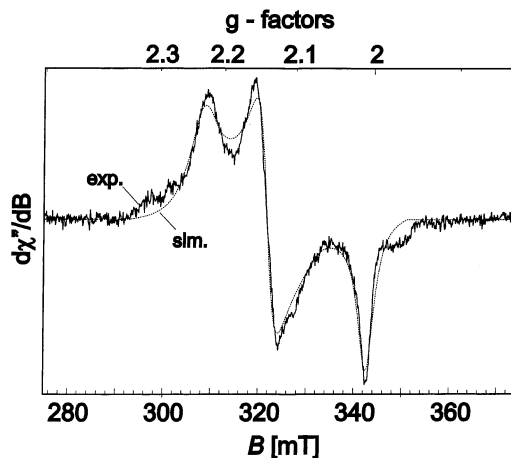
(29) (a) Amos, A. T.; Hall, G. G. *Proc. R. Soc. Ser. A* **1961**, *263*, 483. (b) King, H. F.; Stanton, R. E.; Kim, H.; Wyatt, R. E.; Parr, R. G. *J. Chem. Phys.* **1967**, *47*, 1936.
(30) Sellmann et al. in ref 6 have reported an effective magnetic moment of 1.9 μ_B at 298 K for [Fe(gma)(PCy$_3$)] (Cy = cyclohexanyl), which is too low a value. We have found that the analogous complex **6**, [Fe(gma)(P(*n*-propyl)$_3$)], possesses an S_t = 1 ground state (μ_{eff} = 2.9 μ_B at 298 K).

Figure 2. X-band EPR spectrum of [Fe(gma)I] in frozen pyridine at 20 K. For *g*-values see text. (Conditions: frequency 9.6344 GHz; power 100 μW; modulation 1 mT/100 kHz.)

Table 3. Electronic Spectra of Complexes in CH$_2$Cl$_2$ Solution (20 °C)

complex	λ, nm (ϵ, L mol^{-1} cm^{-1})
1	342 (1.2 × 10^4), 448 (0.6 × 10^4), 534 (0.5 × 10^4), 638 (0.4 × 10^4), 730sh
2[a]	360 (1.35 × 10^4), 440 (0.8 × 10^4), 470sh, 522 (0.5 × 10^4), 610sh, 915 (0.2 × 10^4)
3	not soluble
4	443 (0.5 × 10^4), 500sh, 610sh, 890 (0.16 × 10^4)
5	not soluble
6	450 (0.7 × 10^4), 515 (0.44 × 10^4), 620sh
7[b]	435 (1.3 × 10^4), 490 (1.33 × 10^4), 450sh, 520sh, 545 (0.7 × 10^4)

[a] In pyridine. [b] In toluene.

Dinuclear **1** reacts with [(*n*-Bu)$_4$N]CN in CH$_2$Cl$_2$ solution under an Ar atmosphere yielding a brown/black precipitate of [(*n*-Bu)$_4$N][Fe(gma)(CN)]·1.5CH$_2$Cl$_2$ (**4**·1.5CH$_2$Cl$_2$). Compound **4** displays a ν(CN) stretching frequency in the infrared at 2106 cm^{-1}. From magnetic susceptibility measurements, effective magnetic moments of 2.8 μ_B at 30 K and 3.3 μ_B at 290 K have been calculated. This is indicative of an S_t = 1 ground state as in mononuclear **2** and **6**.

The reaction of **4** with iodine (1:0.5) in CH$_2$Cl$_2$ solution produced a black precipitate of the neutral complex [Fe(gma)-(CN)]·0.5CH$_2$Cl$_2$ (**5**·0.5CH$_2$Cl$_2$). Thus, **4** undergoes a one-electron oxidation. Interestingly, the ν(CN) stretching frequency is observed at 2111 cm^{-1} in **5,** which is very similar to that observed for **4**. Thus this result points to the conclusion that the oxidation of **4** to **5** is not a metal-centered process. Magnetic susceptibility measurements of solid **5** yield effective magnetic moments of 1.7 μ_B at 15 K and 2.0 μ_B at 295 K, indicating an S_t = 1/2 ground state for **5**. This is corroborated by its rhombic X-band EPR signal in frozen dimethylformamide frozen solution at 20 K (g_1 = 2.23, g_2 = 2.12, g_3 = 2.00).

We discovered that **1** (or **2**) can also be oxidized by iodine in CH$_2$Cl$_2$ yielding the black neutral complex [Fe(gma)I] (**3**). Complex **3** possesses an S_t = 1/2 ground state as was judged from the effective magnetic moment of ~1.7 μ_B measured at 295 K. Its rhombic X-band EPR signal at g_x = 2.23, g_y = 2.14, g_z = 2.01 in frozen pyridine solution at 20 K is in accord with this interpretation (Figure 2).

Table 3 summarizes the electronic spectra of complexes **1**−**7** of which those of **3** and **5** could not be recorded due to their

Table 4. Zero-Field Mössbauer Parameters of Complexes at 80 K

complex	δ,[a] mm s^{-1}	$|\Delta E_Q|$,[b] mm s^{-1}	S_t[c]	S_{Fe}[d]	ref
1	0.24	2.01	0	3/2	7
2	0.27	2.33	1	3/2	this work, 7
3	0.27	1.93	1/2	3/2	this work
4	0.18	1.83	1	3/2	this work
5	0.16	1.60	1/2	3/2	this work
6	0.14	2.29	1	3/2	this work
7	0.24	0.98	0	0	this work
[(PhBMA)Fe]	0.45	0.90	1	1	7
[Fe^{II}(L$^{2\bullet}$)(PR$_3$)]	0.04	3.16	0	0	33

[a] Isomer shift vs α-Fe at 298 K. [b] Quadrupole splitting. [c] Ground state of the molecule. [d] Local spin state at the iron ion.

insolubility in all common solvents. It is noted that the observed, intense absorption maxima in the visible are quite similar for complexes **1**, **2**, **4**, and **6**, in agreement with the notion (see below) that they all contain an intermediate spin ferric ion (S_{Fe} = 3/2) and a coordinated radical trianion (gma$^\bullet$)$^{3-}$ as chromophore.

Zero-Field Mössbauer Spectroscopy. Zero-field Mössbauer spectra of polycrystalline samples were recorded at 80 K. The results are summarized in Table 4.

The zero-field Mössbauer spectra of mononuclear **2**−**7** at 80 K each consist of a well-resolved doublet. The spectra recorded previously by Strähle et al.[7] for **1** and **2** are within experimental error identical with our measurements on the same complexes.

It is remarkable, that complexes **1**−**6** display isomer shift values, δ, in the narrow range 0.14−0.27 mm s^{-1} and quadrupole splitting parameters, ΔE_Q, in the range 2.33 to 1.60 mm s^{-1} despite the fact that the species have different ground states, S_t, which vary from 0 in **1** and **7**, to 1/2 in **3** and **5**, and to 1 in **2**, **4**, and **6**.

It is also remarkable, that within redox-related pairs of complexes such as **4** and **5** or **1** and **3** or **2** and **3** the Mössbauer parameters do not vary greatly either. This observation immediately rules out the possibility that one-electron oxidation of **1**, **2**, or **4** is a metal-centered process. It is clear that a consistent description of the electronic structure of complexes **1**−**6** *must involve the same local electronic configuration at the central iron ion in all complexes*. Thus a description of **1** as a low-spin ferrous species (S_{Fe} = 0) and **2** as containing an intermediate-spin ferrous ion (S_{Fe} = 1) is *not* consistent with the Mössbauer data.[7]

In stark contrast, an expansion of the coordination number from five in **6** to six in **7** (one and two phosphines) induces a significant change of the Mössbauer parameters (Table 4). Thus the local electronic structure of the central iron ions cannot be the same in **6** and **7**.

Changing the ligand gma in [Fe(gma)]$_2$ (**1**) by phthaldialdehyde-bis(2-mercaptoanil), (PhBMA)$^{2-}$, in [Fe^{II}(PhBMA)] (S_t = 1)[7] (Scheme 1) brings about a large shift of the isomer shift from 0.24 to 0.45 mm s^{-1} and the quadrupole splitting decreases from 2.01 to 0.90 mm s^{-1}.[7] The complex possesses an S_t = 1 ground state and is probably mononuclear. Here it is conceivable that the oxidation states of the iron ions in both compounds are different. It is significant that [Fe(PhBMA)] with presumably a square-planar ligand field (Fe^{II}N$_2$S$_2$) displays similar Mössbauer parameters as reported for a few square-planar, intermediate-spin ferrous complexes with porphyrin and phthalocyanine
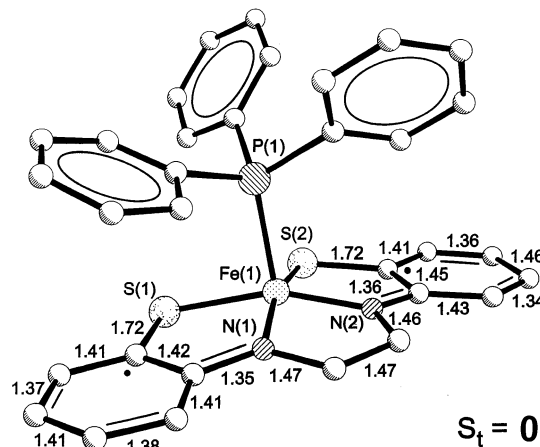
Figure 3. Schematic view of the neutral molecule [FeL(PPh$_3$)] and bond distances (Å); ref 33.

ligands.[31] We have also measured the Mössbauer spectrum of [HNEt$_3$]$_2$[Fe^{II}(o-C$_6$H$_4$S$_2$)$_2$] (S_t = 1), a genuine square-planar, bis(o-dithiolato)iron(II) complex[32] for which the following Mössbauer parameters have been measured at 80 K: δ = 0.44 mm s^{-1}, ΔE_Q = 1.18 mm s^{-1}. These data are very close to the data for [Fe(PhBMA)]. Thus we propose that [Fe^{II}(PhBMA)] is a genuine intermediate spin ferrous species (S_{Fe} = 1). Note the difference in isomer shift and quadrupole splitting on going from [Fe^{II}(PhBMA)] to **2** or **4**, both of which have also an S_t = 1 ground state which is obviously of quite different origin.

Sellmann et al.[33] have reported an analogue of **6** which contains a hydrogenated bridging ligand, LH$_4$ = 1,2-ethanediamine-N,N′-bis(2-benzenethiol), namely, [FeL(P(n-propyl)$_3$)]. This compound and its triphenylphosphine derivative have been structurally characterized (Figure 3) and its Mössbauer spectrum has been reported at 4.2 K: δ = 0.04 mm s^{-1} and ΔE_Q = 3.16 mm s^{-1}. These values differ significantly from those reported here for **6**. We have recently shown that the electronic structure of [FeL(P(n-propyl)$_3$)] is best described as that of a diradical coordinated to a low-spin ferrous ion.[34] The π radicals are clearly identified by X-ray crystallography; they are intramolecularly antiferromagnetically coupled. In contrast to Sellmann's report, we find magnetochemically a singlet (and not as reported a triplet) ground state for [Fe^{II}(L$^{2\bullet}$)(PPh$_3$)] upon repeated fractional recrystallization.[35] The diamagnetic complex [Ru^{II}(L$^{2\bullet}$)(PR$_3$)] is isostructural and possesses also an S_t = 0 ground state.[36]

As stated above, the most remarkable feature of the Mössbauer spectroscopic investigation is the observation that complexes **1**−**6** display very similar Mössbauer parameters: the isomer shift is in the range 0.14−0.27 mm s^{-1} and the quadrupole splitting is quite large: ΔE_Q = 1.60−2.33 mm s^{-1}. Thus the local spin state of the iron ions, S_{Fe}, appears to be the same in these complexes. We propose that S_{Fe} = 3/2, i.e., an

(31) (a) Medhi, O, K.; Silver, J. *J. Chem. Soc., Chem. Commun.* **1989**, 1199. (b) Dale, B. W.; Williams, R. J. P.; Edwards, P. R.; Johnson, C. E. *J. Chem. Phys.* **1968**, *49*, 3445. (c) Labarta, A.; Molins, E.; Vinas, X.; Tejada, J.; Caubet, A.; Alvarez, S. *J. Chem. Phys.* **1984**, *80*, 444.
(32) Sellmann, D.; Kleine-Kleffmann, U.; Zapf, L.; Huttner, G.; Zsolnai, L. *J. Organomet. Chem.* **1984**, *263*, 321.
(33) Sellmann, D.; Emig, S.; Heinemann, F. W.; Knoch, F. *Angew. Chem.* **1997**, *109*, 1250. Sellmann, D.; Emig, S.; Heinemann, F. W.; Knoch, F. *Angew. Chem., Int. Ed. Engl.* **1997**, *36*, 1201.
(34) Herebian, D.; Bothe, E.; Bill, E.; Weyhermüller, T.; Wieghardt, K. *J. Am. Chem. Soc.* **2001**, *123*, 10012.
(35) Ghosh, P.; Wieghardt, K., unpublished results.
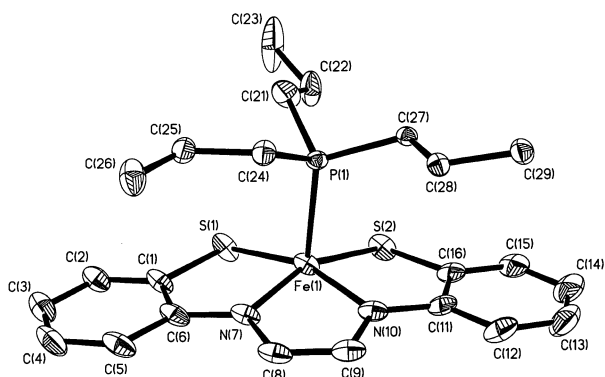(36) Sellmann, D.; Ruf, R.; Knoch, F.; Moll, M. *Inorg. Chem.* **1995**, *34*, 4745.

Figure 4. Structure of the neutral molecule in crystals of **6**.

intermediate spin central ferric ion, prevails. This is corroborated by the fact that the five-coordinate complexes **A**[37] and **B**,[38] having each an $S_{Fe} = 3/2$ ground state, possess the following Mössbauer parameters at 77 and 120 K, respectively: **A**, $\delta = 0.30$ mm s^{-1}; $\Delta E_Q = 3.5$ mm s^{-1}; **B**, $\delta = 0.18$ mm s^{-1}; $\Delta E_Q = 3.56$ mm s^{-1}.
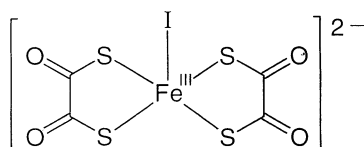
A
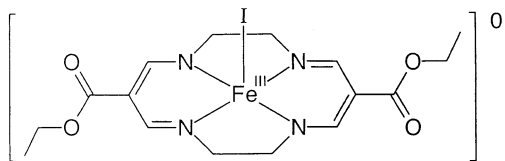
B

Crystal Structures. The crystal structures of **1**[6] and **2**[7] have been reported previously. For the following discussion we present the structural data of the Fe(gma) unit of both complexes in Table 2. We have determined the crystal structure of **6**; the results are also summarized in Table 2, and Figure 4 gives an ORTEP representation of the neutral molecule in crystals of **6**.

Complexes **1**, **2**, and **6** are the only structurally characterized transition-metal complexes containing a tetradentate (gma) ligand. Since it was suspected that this ligand is not as redox innocent as assumed by all previous researchers, who have always assumed a closed-shell dianion (gma)$^{2-}$ to be present, it would have been illuminating to have the geometrical details of [Zn^{II}(gma)] available as a benchmark for a true (gma)$^{2-}$ dianion. Since these are not available, we have calculated its structure using density functional theory (see below). The results are summarized in Figure 5.

The most salient feature of the three crystal structure determinations is the observation that the Fe(gma) unit exhibits, within experimental error, the same structural details. The Fe–N, Fe–S, C–C, C–N, and C–S bond distances are nearly identical in all three structures. It is also significant that the
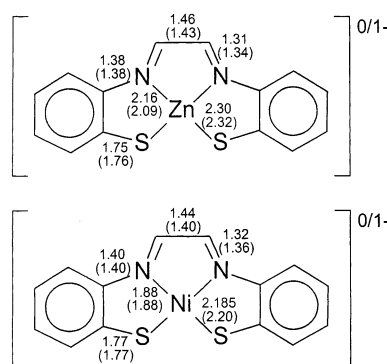
(37) Nicarchos, D.; Kostikas, A.; Simopoulos, A.; Coucouvanis, D.; Piltingsrud, D.; Coffman, R. E. *J. Chem. Phys.* **1978**, *69*, 444.
(38) Keutel, H.; Käpplinger, I.; Jäger, E.-G.; Grodzicki, M.; Schünemann, V.; Trautwein, A. X. *Inorg. Chem.* **1999**, *38*, 2320.

Figure 5. Schematic view of the calculated structures of [Zn(gma)], [Ni-(gma)], and (in brackets) [Ni(gma$^\bullet$)]$^-$ and [Zn(gma$^\bullet$)]$^-$. Bond distances are in angstroms.

[Li(Bu$^t_2$DAB)$_2$]   (S_t = ½)

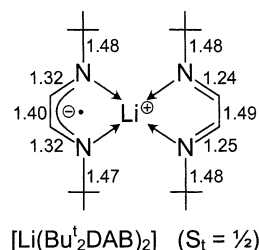**Figure 6.** Schematic view of [Li(Bu$^t_2$DAB)$_2$] from ref 39. Bond distances are given in angstroms.

two six-membered rings in the gma units possess each six nearly equidistant C–C bonds contrasting in this respect the structure of [FeL(PPh$_3$)] shown in Figure 3. Thus the *o*-iminothiophenolate part of (gma) is aromatic. We have not discovered any evidence for a quinoid-type distortion with two short C=C bonds and four longer ones as has been reported for a number of coordination compounds containing *o*-iminothiobenzosemiquinonate(1−) π radicals.[34]

It is the glyoxal bridging unit of gma which displays some unusual features: (i) The C–C bond at ~1.38 Å is far too short for a C–C single bond between two sp^2-hybridized carbon atoms. (ii) Correspondingly, the two C=N bonds of the α-diimine part of gma at ~1.35 Å are too long for genuine C=N double bonds. Interestingly, in the calculated structure of [Zn(gma)] these bonds are more in line with a closed-shell dianion: the central C–C bond is longer at 1.46 Å and the two C=N bonds are shorter at 1.31 Å (Figure 5). Thus, the structural parameters indicate that in complexes **1**, **2**, and **6** the trisanionic radical (gma$^\bullet$)$^{3-}$ is coordinated to a ferric ion, whereas in [Zn-(gma)] the closed-shell dianion is bound to a Zn(II) ion.

These structural results and their interpretation are nicely corroborated by a crystallographic study on paramagnetic bis-(1,4-di-*tert*-butyl-1,4-diazabutadiene) adducts of lithium, magnesium, and zinc by Raston et al.[39] Figure 6 shows a representation of the structure of [Li(Bu$^t_2$DAB)$_2$] ($S = 1/2$) which contains a closed-shell neutral ligand and an open-shell radical anion both N,N-coordinated to a lithium cation. The C–N and C–C distances in the ligands are significantly different in their neutral and monoanionic forms. The comparable C=N and C–C bond lengths in **1**, **2**, and **6** resemble closely those of the radical anion in [Li(Bu$^t_2$DAB)$_2$]. Thus we propose that the electronic structure of **1** should be described as [Fe^{III}(gma$^\bullet$)]$_2$, that of **2** as

(39) Gardiner, M. G.; Hanson, G. R.; Henderson, M. J.; Lee, F. C.; Raston, C. L. *Inorg. Chem.* **1994**, *33*, 2456.

Table 5. Calculated Structural Parameters for the Complexes of This Study[a]

|	M_S	M–N	M–S	M–X	C15–C16[b]	C15–N1[b]	C1–S1[b]	C6–N1[b]
[Zn(gma)]	0	2.158	2.296		1.463	1.309	1.746	1.380
[Zn(gma)]	1	2.068	2.320		1.416	1.353	1.744	1.366
[Zn(gma•)]⁻	1/2	2.092	2.315		1.429	1.340	1.761	1.380
[Ni(gma)]	0	1.883	2.185		1.437	1.321	1.768	1.408
[Ni(gma)]	1	1.877	2.160		1.393	1.364	1.768	1.385
[Ni(gma)]	0 (bs)	1.879	2.159		1.395	1.361	1.767	1.384
[Ni(gma•)]⁻	1/2	1.881	2.196		1.402	1.357	1.772	1.396
[Fe(gma•)(py)]	1 (bs)	1.918	2.215	1.997	1.396	1.362	1.775	1.402
exptl		1.904	2.216	2.076	1.382	1.336	1.755	1.408
[Fe(gma•)(PH₃)]	1 (bs)	1.906	2.220	2.216	1.393	1.369	1.776	1.405
exptl		1.883	2.199	2.318	1.354	1.375	1.765	1.398
[Fe(gma•)(CN)]⁻	1 (bs)	1.904	2.211	1.915	1.384	1.373	1.767	1.395
[Fe(PhBMA)]	1	1.956	2.226			1.324	1.758	1.430
[Fe(gma)(PH₃)₂]	0 (bs)	1.911	2.312	2.203/2.245	1.432	1.340	1.753	1.414
[Fe(gma)(py)]⁺	1/2 (bs)	1.936	2.251	2.128	1.386	1.361	1.747	1.382
[Fe(gma)(CN)]	1/2 (bs)	1.921	2.167	1.865	1.415	1.340	1.787	1.411
[Fe(gma)(Cl)]	1/2 (bs)	1.927	2.187	2.187	1.412	1.339	1.778	1.405
[Fe(gma)I]	1/2 (bs)	1.923	2.180	2.545	1.411	1.341	1.779	1.401

[a] Distances are in angstroms. M = metal (Zn, Ni, Fe); X = axial ligand (py, PH₃, CN⁻, Cl⁻, I⁻); bs = broken symmetry. [b] Labeling as in Table 2.

[Fe^{III}(gma•)(py)]·py, and that of **6** as [Fe^{III}(gma•)(P(*n*-propyl)₃)]. In contrast, in the calculated structure of [Zn(gma)] these C—C and C=N distances resemble more closely those of the neutral ligand in [Li(Bu^{t}₂DAB)₂], indicating the expected electronic structure of a divalent zinc ion and of an N,N-coordinated closed-shell dianion (gma)²⁻.

DFT Calculations. In this section a detailed picture of the electronic structure of complexes [M(gma)(X)$_m$]^n (M = Zn, Ni, Fe; X = py, PH₃, CN⁻, I⁻; *m* = 1, 2; *n* =0, −1, +1) will be given on the basis of DFT calculations. The emphasis of the calculations is to generate an experimentally calibrated bonding scheme that provides an intuitive understanding of this fascinating class of substances. In order of increasing electronic structure complexity, we will first discuss [Zn(gma)]$^{0,−}$ then [Ni(gma)]$^{0,−}$, and finally the iron complexes that show an enormous diversity in their electronic structures.

Zn Complexes. The most straightforward complex in the series is [Zn(gma)], which is diamagnetic; a closed-shell Zn-(II) ion (d^{10}) is bound to a closed-shell ligand. The calculated structure features fairly long Zn—N and Zn—S distances (Figure 5 and Table 5). The most interesting bonds are within the α-diimine linkage where the C—C distance is 1.463 Å and the C—N distance is 1.309 Å. The C—C distance is a bit too short for a true single bond and the C—N distance is a bit too long for a double bond, in agreement with the calculated Löwdin bond orders of 1.19 and 1.75, respectively. The distances within the aromatic rings show essentially equivalent C—C distances for all complexes of this study and will not be discussed further. It clearly shows the absence of benzosemiquinonato π-radical character in this part of the ligand (gma)²⁻ or (gma)³⁻.

The MO diagram of [Zn(gma)], however, shows a remarkable feature—the gap between the HOMO and LUMO shown in Figure 7 is only ∼0.25 eV (∼2000 cm⁻¹) at the BP86 level.[42] In the C_{2v} point group these orbitals transform as a₂ and b₂ respectively and will be referred to as L(a₂) and L(b₂), respectively (Figure 7). The HOMO mainly represents the antisymmetric combination of the two thiolate out-of-plane lone
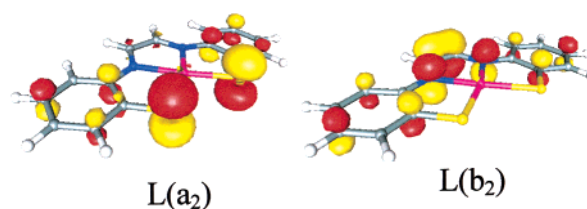
Figure 7. HOMO L(a₂) and LUMO L(b₂) of **8**.

pairs which show, however, some conjugation into the ring systems. The LUMO on the other hand is mainly located on the α-diimine unit and is bonding between the carbons and antibonding between the nitrogens (Figure 7). *This LUMO is exceptionally low in energy and it is this feature which gives exceptional properties to the whole series of complexes studied in the present work.*

The energetic closeness of the HOMO and LUMO in [Zn-(gma)] implies that: (a) the first excited triplet state should be low in energy and (b) its one-electron reduction should be fairly easy. There is no experimental value for the singlet—triplet separation. However, the adiabatic excitation energy calculated at the B3LYP level gives a reasonable value of 13.8 kcal/mol (4850 cm⁻¹), which would fall into the near-IR region of the spectrum. Thus, the first triplet state is indeed low in energy. The calculated structure shows that that the main changes upon depopulating the HOMO and populating the LUMO occur within the α-diimine linkage where the C—C bond shrinks by ∼0.05 Å and the C—N bonds expand about the same amount. Both of these changes are consistent with the shape of the LUMO that is C—C bonding and C—N antibonding.

The anion [Zn(gma•)]⁻ has been prepared and characterized by Maki et al.[2d] The calculations show that the extra electron enters the LUMO of [Zn(gma)] to give [Zn(gma•)]⁻. As

(40) Szabo, A.; Ostlund, N. S. *Modern Theoretical Chemistry*; MacMillan Pub. Inc.: New York, 1982.

(41) (a) Petersilka, M.; Gossmann, U. J.; Gross, E. K. U. *Phys. Rev. Lett.* **1996**, *76*, 1212. (b) Petersilka, M.; Gross, E. K. U. *Int. J. Quantum Chem.* **1996**, *30*, 181. (c) Görling, A. *Phys. Rev. Lett.* **1996**, *54*, 3912.

(42) Note that orbital energy differences are more meaningful in DFT calculations that do not incorporate the Hartree—Fock exchange compared to those calculated with hybrid functionals or the Hartree—Fock method. In HF calculations the virtual orbitals "see" and *N* electron system instead of a *N* − 1 electron system as it should be.[40] Therefore all of these orbitals are too high in energy and are too diffuse. To the extent that HF exchange is incorporated into hybrid DFT, this shortcoming is "inherited" from HF in these functionals. There are no observables that can be meaningfully related to the orbital energy differences in either case. By contrast, for "pure" functionals the virtual orbitals are appropriate and the orbital energy differences are well-defined zero-order approximations for excitation energies.[41]

expected, upon reduction the C−C bond of the α-diimine linkage shrinks and the C−N distances increase analogously to the results found for the triplet state of [Zn(gma)]. Evidently, it is the population of the LUMO orbital which is responsible for these systematic structural changes. It was shown that the EPR *g*-values of [Zn(gma•)]⁻ are very close to the free-electron *g*-value (g_{iso} = 2.0027).[2d] Nitrogen hyperfine couplings were apparently not observed in this early work. Using recently developed methods,[10,11] we have calculated the *g*-values and nitrogen hyperfine couplings for [Zn(gma•)]⁻ at the B3LYP level. We obtain *g*-values of 2.001, 2.0025, and 2.0035, which are fully consistent with experiment. The computed hyperfine couplings for the two equivalent nitrogens amount to 27, −3, and −3 MHz (isotropic and dipolar parts considered), and the Zn ion shows very small couplings of −2 MHz (isotropic, dipolar, and second-order spin−orbit coupling (SOC) parts considered). All of these values are consistent with the experimental spectra and unequivocally confirm the contention of Maki et al. that [Zn(gma•)]⁻ can only be reasonably formulated as a closed-shell d^{10} anion coordinated to the trianionic radical form of the ligand gma, i.e., (gma•)³⁻. It is also clear from the shape of the LUMO, which also dominates the spin density distribution (not shown), that the SOC of the heavier sulfur atoms will have essentially no influence on the observed *g*-tensor to any significant extent as has been conjectured by Maki et al.[2d]

In summary, the calculations on [Zn(gma)] and [Zn(gma•)]⁻ show that the gma ligand features an extremely low-lying LUMO orbital which is mainly centered on the α-diimine linkage and which makes the ligand fairly electrophilic. Consequently, the first excited triplet state is energetically close to the ground state and the reduction of the ligand proceeds fairly easily. The C−C and C−N distances of the α-diimine unit are the structural markers for the occupation of the LUMO orbital. *C−C distances of shorter than* ∼1.42 Å *and C−N distances longer than* ∼1.33 Å indicate that the LUMO is occupied irrespective of whether the HOMO (L(a₂)) is occupied by one or two electrons.

Ni Complexes. The corresponding Ni(II) complexes [Ni-(gma)] and [Ni(gma•)]⁻ have also been prepared and characterized by a number of workers,[2] but a crystal structure is not available. We have therefore calculated the structure of [Ni-(gma)] in the closed-shell $S = 0$, in the $S = 1$, and in the broken-symmetry $M_S = 0$ state. The calculations at the B3LYP level show that the closed-shell state is lowest in energy, followed by the very low-lying triplet state at 3.4 kcal/mol and the BS state at 5.0 kcal/mol. The closed-shell ground state is in agreement with the observed diamagnetism of [Ni(gma)]. The optimized structure of [Ni(gma)] shows an α-diimine C−C distance of 1.437 Å and a C−N distance of 1.321 Å, which suggests that gma is coordinated in its dianionic, closed-shell form in [Ni(gma)]. This conclusion is fully confirmed by the MO's found in the upper valence region of [Ni(gma)]. The orbital plots show a doubly occupied HOMO and an unoccupied LUMO, both of which closely match the corresponding orbitals of [Zn(gma)] (Figure 7). Above the LUMO there is a mainly Ni-centered $d_{x^2-y^2}$ based orbital which is strongly σ-antibonding with the ligands (Figure 8). To lower energy than the HOMO one finds four mainly Ni 3d-based orbitals that are all doubly occupied. Thus, the electronic structure of [Ni(gma)] is best
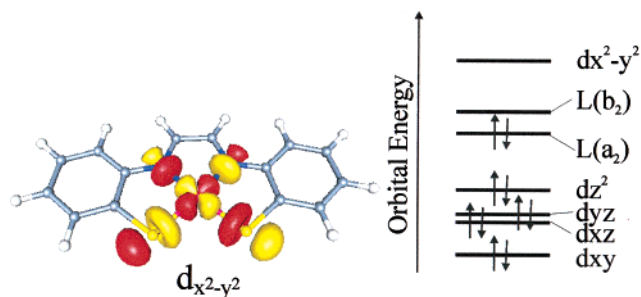

Figure 8. Ni $d_{x^2-y^2}$ based LUMO+1 of [Ni(gma)] and a qualitative MO level scheme.
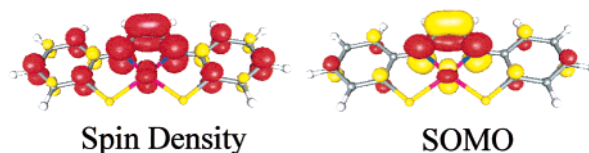

Figure 9. Total spin density (left, red = positive spin density, yellow = negative spin density) and the singly occupied natural orbital (right) of [Ni(gma)]⁻.

described as a low-spin d^8 Ni(II) coordinated to a closed-shell (gma)²⁻ ligand. The electronic configuration is thus $(d_{xy})^2(d_{xz})^2$-$(d_{yz})^2(d_{z^2})^2(L(a_2))^2(L(b_2))^0(d_{x^2-y^2})^0$ (Figure 8).

The anion of [Ni(gma•)]⁻ can be easily prepared electrochemically or chemically with Na/Hg in methyltetrahydrofuran. Its EPR properties have been reported, but the interpretation of the EPR parameters was found to be difficult because they deviate from that of [Zn(gma•)]⁻.[2d] The plausible reasoning was that if both [Zn(gma•)]⁻ and [Ni(gma•)]⁻ feature the same (gma•)³⁻ radical ligand and a closed-shell M(II) ion, their EPR spectra should be fairly similar. However, [Ni(gma•)]⁻ shows a much larger *g*-anisotropy than [Zn(gma•)]⁻, with observed *g*-values of 1.975, 2.005 and 2.026. These values vary in the third decimal with the solvent used.[2d] The observed anisotropy is apparently too large for standard organic radicals and too small for a true Ni(III) or Ni(I) species. It is also noteworthy that one of the *g*-values is below the free electron *g*-value which is uncommon. Again, however, the *g*-tensor of [Ni(gma•)]⁻ finds a concise explanation from the B3LYP DFT calculations. The calculated total spin density distribution and the singly occupied natural orbital of [Ni(gma•)]⁻ are shown in Figure 9. It is obvious that they mainly reflect the shape of the L(b₂) LUMO with some additional spin polarization, which accounts for the negative spin densities observed within the rings. However, in contrast to [Zn(gma•)]⁻ there is also some spin density located on the central Ni, which amounts to ∼10% according to our B3LYP results. This spin density results from the interaction of the Ni d_{yz} orbital with L(b₂), which is allowed by symmetry.

The antibonding nature of the SOMO depicted in Figure 9 indicates that it results from the interaction of a lower lying doubly occupied d_{yz} orbital with the higher lying empty L(b₂). It therefore corresponds to the transfer of electron density from the metal to the ligand and should be viewed as a back-bonding interaction. The reason this interaction occurs in [Ni(gma•)]⁻ but not in [Zn(gma•)]⁻ may be interpreted as follows: (1) the metal−ligand distances are much shorter in [Ni(gma•)]⁻ than in [Zn(gma•)]⁻ (Table 5). This simply is a consequence of having the strongly σ-antibonding $d_{x^2-y^2}$ based MO doubly occupied in [Zn(gma•)]⁻, but empty in [Ni(gma•)]⁻. However,

due to the closer contact a stronger metal−ligand interaction results in [Ni(gma•)]⁻.[2] The 3d manifold is certainly lying at considerably deeper energies for Zn(II) compared to Ni(II) due to the higher effective nuclear charge seen by the 3d electrons in Zn(II). Therefore, the Zn(II) 3d-orbitals are much less available for back-bonding than the Ni(II) orbitals.

The out-of-plane spin density in a π-orbital of the central Ni ion also nicely explains the pattern of g-values with one g-value significantly above the free electron g-value and one g-value below it. The positive g-shift arises from the SOC interaction between the spin-carrying Ni d_{yz} orbital and the doubly occupied Ni d_{xz} orbital, which gives an angular momentum along the normal of the complex plane. By contrast, the SOC between the Ni d_{yz} orbital and the empty Ni $d_{x^2-y^2}$ orbital results in an angular momentum along the x-direction and a negative g-shift. The third g-shift occurs along the y-direction and arises from the interaction with the d_{xy} orbital, which is filled and much lower in energy. Therefore this g-shift is expected, calculated, and observed to be close to the free-electron g-value.

Given the calculated spin density, the calculated g-values become at the B3LYP level 1.965 (perpendicular to the complex plane), 2.005, and 2.033 (in the complex plane). The increased g-shifts of [Ni(gma•)]⁻ relative to [Zn(gma•)]⁻ are due to the enhanced angular momentum in the ground state that enters through the small amount of SOC at the metal into the ground-state wave function. Thus, the calculations account accurately for the experimental findings and explain the interesting differences in the EPR properties of [Zn(gma•)]⁻ and [Ni(gma•)]⁻. For completeness, we also note the calculated nitrogen hyperfine couplings, which are 31, −2, and −2 MHz, respectively, along the g-tensor main axes. The calculated ⁶¹Ni hyperfine couplings are fairly small and amount to −11, −8, and 4 MHz, which will be difficult to observe.

Finally, we wish to comment on the observed difference in the electrochemical properties of [Zn(gma)] and [Ni(gma)]. It was observed by Maki et al.[2d] that [Ni(gma)] is reduced to [Ni(gma•)]⁻ at a potential of −0.41 V (vs saturated calomel in DMF), whereas the reduction takes place at −0.92 V in [Zn-(gma)] under identical conditions. This has been interpreted as strong evidence against similar electronic structures in [Zn(gma)] and [Ni(gma)], which is *not* consistent with our interpretation. However, this result is easily explained on the basis of our calculations—since the $d_{x^2-y^2}$ based MO is empty in [Ni(gma)] and fully occupied in [Zn(gma)], there is a large difference in charge donation from the ligand to the metal. In the case of [Ni(gma)] there is a large ligand-to-metal charge donation via the fully occupied bonding partner of the strongly σ-antibonding $d_{x^2-y^2}$ based MO. In [Zn(gma)] this charge donation is eliminated because the antibonding $d_{x^2-y^2}$ based MO is fully occupied, thus leading to essentially no or very little charge donation to the central Zn(II). Consequently, the gma ligand is expected to have a considerably higher electron affinity in [Ni(gma)], which is consistent with the experimental observations.

In summary, the appropriate electronic structure description for [Ni(gma•)]⁻ is a closed-shell Ni(II) ion bound to a (gma•)³⁻ trianionic radical with the electronic configuration $(d_{xy})^2(d_{xz})^2$-$(d_{yz})^2(d_{z^2})^2(L(a_2))^2(L(b_2))^1(d_{x^2-y^2})^0$. This description is borne out by the analysis of its EPR parameters of [Ni(gma•)]⁻ and is also clearly reflected in the structural parameters of the α-diimine unit (Table 5).
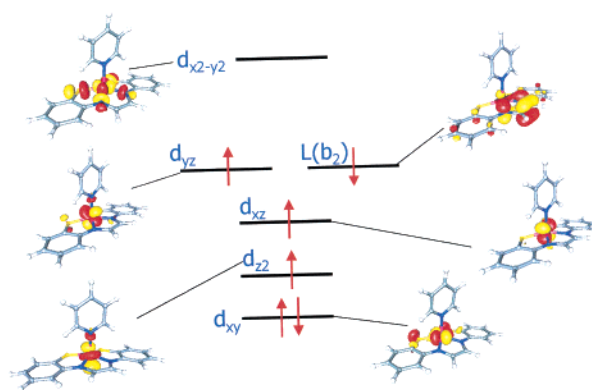
Figure 10. Qualitative bonding scheme for [Fe(gma)(py)] as derived from BS-B3LYP DFT calculations. The doubly occupied MO's are canonical MO's and the singly occupied MO's result from a corresponding orbital transformation.

Iron Complexes. The most interesting and diverse group of complexes studied in this work are the iron complexes. The interpretation of their electronic structures is fairly involved and was only achieved in a consistent fashion through the ability of reliably predicting the Mössbauer parameters by DFT[12] together with the possibility of obtaining quasi-valence bond type wave functions from Noodleman's BS approach.[43] As will be discussed at length elsewhere this approach is expected to yield rather accurate charge densities but unphysical spin densities. Since the Mössbauer isomer shift and quadrupole splitting depend only on the total charge density, they can be reliably and efficiently predicted by BS DFT calculations in spin-coupled systems.

a. Electronic Structure of [Fe(gma)(py)], [Fe(gma)(CN)]⁻, and [Fe(gma)(PR₃)]. The first group of related complexes are the compounds [Fe(gma)(py)], [Fe(gma)(PR₃)] (PR₃ is modeled as PH₃ in the calculations), and [Fe(gma)(CN)]⁻. All of these complexes exhibit an $S = 1$ ground state and comparable Mössbauer parameters. We will analyze the electronic structure of [Fe(gma)(py)] in detail. The results for [Fe(gma)(CN)]⁻ and [Fe(gma)(PR₃)] are similar.

The calculations show that the lowest energy spin-unrestricted solution with $M_S = 1$ is of the BS type. A qualitative bonding scheme derived from these calculations is shown in Figure 10. One finds four occupied orbitals that are mainly iron in character. One of these orbitals is labeled d_{xy} and is found in the spin-up as well as in the spin-down set of orbitals and is therefore doubly occupied. The three other iron-based orbitals are labeled d_{xy}, d_{yz}, and d_{z^2} and only occur in the spin-up manifold. These orbitals are therefore singly occupied with parallel spins. The fifth orbital of the iron 3d manifold, $d_{x^2-y^2}$, is found to be empty for both spin orientations. This orbital occupation pattern defines an intermediate-spin Fe(III) config-uration at the iron site ($S_{Fe} = 3/2$), as has been conjectured from the Mössbauer data (see above). To arrive at a total M_S of 1, there must be one ligand-based orbital that is occupied in the spin-down manifold and empty in the spin-up manifold. This orbital closely corresponds to L(b₂), the α-diimine based LUMO of the ligand in all three complexes. *Thus, the basic electronic description features an intermediate-spin Fe(III) which is strongly antiferromagnetically coupled to a (gma•)³⁻ radical.*

(43) (a) Noodleman, L. *J. Chem. Phys.* **1981**, *74*, 5737. (b) Noodleman L.; Davidson, E. R. *Chem. Phys.* **1986**, *109*, 131.

This amounts to an intramolecular electron transfer from Fe-(II) to the ligand.

For the analysis of the spin coupling it is advantageous to change to an alternative set of MO's, i.e., the corresponding orbitals.[29] This set of orbitals shows most clearly the involved spin couplings, since it will transform the orbitals in the spin-up and the spin-down sets such that the most similar possible pairs result. In practice this means that one finds spin-up and spin-down pairs with an overlap of essentially unity (within $10^{-3}-10^{-4}$), one spin-coupled pair with an overlap between 0 and unity, and two spin-up orbitals that are not matched by occupied spin-down orbitals, since there are two spin-up electrons in excess for a $M_S = 1$ determinant. The two unmatched orbitals are located on the iron and are labeled d_{xz} and d_{z^2} in Figure 10. The larger the overlap within the spin-coupled pair, the stronger the electronic coupling between the spin-carrying fragments. In the present case the spin-coupled ("magnetic") pair is formed between the iron d_{yz} based MO and the $L(b_2)$ α-diimine LUMO orbital as depicted in Figure 10. The mutual overlap of these two orbitals is 0.626, which indicates a strong interaction. The exchange interaction parameter which is best estimated through Yamaguchi's formula (eq 1,[44] $\hat{H}_{HDvV} = -2J\hat{S}_A\hat{S}_B$) is calculated to be -1142 cm^{-1}:

$$J = -\frac{E_{HS} - E_{BS}}{\langle S^2 \rangle_{HS} - \langle S^2 \rangle_{BS}} \quad (1)$$

Note that the spin-expectation value is directly related to the corresponding orbital overlap eq 2:

$$\langle S^2 \rangle_{BS} = \left(\frac{N^\alpha - N^\beta}{2}\right)\left(\frac{N^\alpha - N^\beta}{2} + 1\right) + N^\beta - \sum_i n_i^\alpha n_i^\beta |S_{ii}^{\alpha\beta}|^2 \quad (2)$$

where $N^{\alpha,\beta}$ are the number of spin-up and spin-down electrons, $n_i^{\alpha,\beta}$ are the individual spin-up and spin-down occupation numbers, and the sum over i extends over the corresponding orbital pairs with $S_{ii}^{\alpha\beta}$ being the spatial overlap integral for the ith pair. In the present case we have one "magnetic" pair and therefore $\langle S^2 \rangle_{BS} = S(S + 1) + 1 - |S_{ii}^{\alpha\beta}|^2$. In the strong interaction limit $S_{ii}^{\alpha\beta} \rightarrow 1$ and the BS solution represents a pure spin state. In the weak interaction limit $S_{ii}^{\alpha\beta} \rightarrow 0$ and the BS state represents a mixed spin state which would require a multideterminant wave function in a more concise electronic structure description. However, eq 1 involving the spin expectation values takes neatly care of the two interaction extremes and has been shown to be a reasonable approximation over the whole domain of interaction strengths.[44] The strength of the antiferromagnetic interaction is reflected in the value $|S_{ii}^{\alpha\beta}|^2$ and in addition, by looking at the shape of the overlapping "magnetic pair" one can gain insight into the "pathway" for antiferromagnetic coupling (at least to the extent that such a thing as an "exchange pathway" exists).

In the present case the result of the corresponding orbital analysis is that there is a strong antiferromagnetic exchange interaction between the (gma•)³⁻ ligand and the central iron via a π-overlap pathway to produce the electronic configuration

Table 6. Calculated (B3LYP DFT method) and Experimental Mössbauer Parameters for the Iron Complexes Studied in This Work[a]

	M_S	δ (mm/s)	ΔE_Q (mm/s)	η
[Fe(gma•)(py)]	1 (bs)	0.205	2.371	0.084
exp.	1	0.27	2.33	n.d.
[Fe(gma•)(PH₃)]	1 (bs)	0.142	2.209	0.042
exp.	1	0.14	2.29	n.d.
[Fe(gma•)(CN)]⁻	1 (bs)	0.057	1.787	0.095
exp.	1	0.18	1.83	n.d.
[Fe(PhBMA)]	1	0.419	2.218	0.284
exptl	1	0.45	0.90	n.d.
[Fe(gma)(PH₃)₂]	0 (bs)	0.318	0.779	0.918
exptl	0	0.24	0.98	n.d.
[Fe(gma)(py)]⁺	1/2 (bs)	0.246	2.430	0.023
	3/2	0.253	2.969	0.170
[Fe(gma)(CN)]	1/2 (bs)	0.035	2.618	0.105
exptl	1/2	0.16	1.63	n.d.
[Fe(gma)(Cl)]	1/2 (bs)	0.131	2.629	0.089
[Fe(gma)I]	1/2 (bs)	0.136	2.718	0.088
exptl	1/2	0.27	2.33	n.d.

[a] n.d. = not determined; bs = broken symmetry.

$(L(a_2))^2(d_{xy})^2(d_{xz})^1(d_{yz})^1(d_{z^2})^1$ $(L(b_2))^1(d_{x^2-y^2})^0$. This electronic configuration indicates that, compared to [Ni(gma)], the iron orbitals are higher in energy and readily lead to a one-electron reduction of the ligand. This is consistent with the considerably lower effective nuclear charge of Fe(II) compared to Ni(II) as may be derived from X-ray absorption spectra on divalent metal chloride species.[45]

The calculated strong exchange interaction is consistent with the observed "pure" spin of $S = 1$ with no indication of thermal population of the higher lying $S = 2$ state up to room temperature. However, since the precise value of J is not known from experiment, the accuracy of the calculation cannot be checked.

A much more accurate check on the validity of the computational approach is provided by the calculated Mössbauer parameters in relation to experiment (Table 6). A qualitatively erroneous electronic structure description would immediately destroy the agreement between calculated and experimental values. However, in the present case the agreement between theory and experiment is excellent for both, the isomer shift as well as for the quadrupole splitting (Table 6) in the case of [Fe(gma)(py)] and [Fe(gma)(PH₃)]. For the cyanide complex. [Fe(gma)(CN)]⁻, the calculated isomer shift is significantly too small. We have verified that the BS solution found for [Fe(gma)(CN)]⁻ still follows the same pattern as observed for [Fe(gma)(py)] and [Fe(gma)(PH₃)]. Since strong back-bonding tends to reduce the isomer shifts,[46] it is possible that the calculations overestimate the amount of back-bonding to the axial CN⁻ in [Fe(gma)(CN)]⁻. The calculated quadrupole splitting is nevertheless in excellent agreement with the experimental values.

The trend in the observed isomer shift may be explained on the basis of our previous work, which showed that back-bonding interactions between the iron and its ligands will decrease the isomer shift.[46] In the present case both PR₃ and CN⁻ are certainly more strongly back-bonding than pyridine, although the amount of back-bonding will be rather limited due to the

(44) (a) Yamaguchi, K.; Takahara, Y.; Fueno, T. In: *Applied Quantum Chemistry*; Smith, V. H., Eds.; Reidel: Dordrecht, 1986; p 155. (b) Soda, T.; Kitagawa, Y.; Onishi, T.; Takano, Y.; Shigeta, Y.; Nagao, H.; Yoshioka, Y.; Yamaguchi, K. *Chem. Phys. Lett.* **2000**, *319*, 223.

(45) Shadle, S. E.; Hedman, B.; Hodgson, K. O.; Solomon, E. I. *J. Am. Chem. Soc.* **1995**, *117*, 2259.
(46) Li, M.; Bonnet, D.; Bill, E.; Neese, F.; Weyhermüller, T.; Blum, N.; Sellmann, D.; Wieghardt, K. *Inorg. Chem.* **2002**, *41*, 3444−3456.
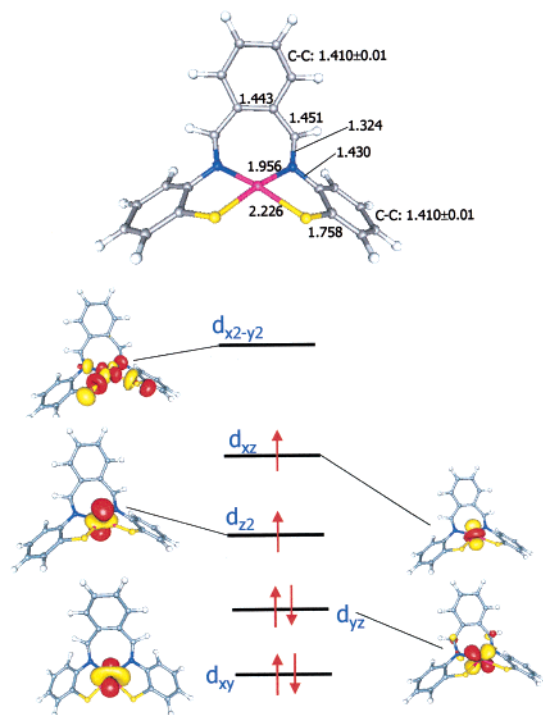
Figure 11. Calculated structure (top, distances in Å) and qualitative bonding scheme (bottom) for [Fe(PhBMA)]. The orbitals result from a spin-unrestricted B3LYP calculations. Doubly occupied MO's are Pipek-Mezey localized MO's, singly occupied MO's are natural orbitals, and the virtual MO is the spin-up LUMO.

ferric oxidation state of the central iron. Nevertheless, the observed isomer shifts for [Fe(gma)(CN)]⁻ and [Fe(gma)(PR₃)] are, as expected, smaller than for [Fe(gma)(py)] (Table 4).

On the basis of these results, we strongly feel that the electronic structure description offered by the calculations is essentially correct. This is also supported by the fairly reasonable agreement between experimental and theoretical structure parameters (Table 5). The only significant deviations occur for the bonding distance to the axial ligands which appear to be significantly underestimated by the calculations but may also be affected experimentally by crystal packing effects.

b. Electronic Structure of [Fe(PhBMA)]. As a check on the validity of the claim that the low lying LUMO of the α-diimine unit is responsible for the unique properties of the series of complexes, we carried out calculations for [Fe-(PhBMA)] which also possesses an $S = 1$ spin state but exhibits quite different Mössbauer parameters[7] *and lacks an α-diimine structural motif.*

Calculations were carried out for $M_S = 0$, $M_S = 1$, and $M_S = 2$ with the lowest energy found for the $M_S = 1$ structure, which is in agreement with the experimental observation. The calculated structure and the calculated bonding scheme are indicated in Figure 11.[47] The calculations clearly show, that [Fe(PhBMA)] does *not* involve any unpaired electrons on the ligand. Instead it features a genuine intermediate spin Fe(II) ion in a four coordinated essentially square planar ligand field. This ligand field leaves the Fe d_{xy} based orbital low in energy, leading to

(47) The shapes of the MO's in Figure 11 do not resemble the textbook-like d-orbitals well. This is a result of the localization procedure used to "separate" the metal from the ligand orbitals. The canonical orbitals are very strongly mixed and are not illuminating in indicating the electronic configuration of the iron. The resulting description we develop here is nevertheless valid.

double occupation and the Fe $d_{x^2-y^2}$ based MO too high in energy to be occupied. Of the remaining iron-based orbitals the calculations predict the Fe d_{yz} based orbital to become doubly occupied. For the remaining two electrons it is energetically more favorable to enter the energetically close lying Fe d_{xz} and Fe d_{z^2} based orbitals rather than to pay the energetic price of spin pairing into one of them. This finally leads to an intermediate spin configuration $(d_{xy})^2(d_{yz})^2(d_{z^2})^1(d_{xz})^1$ at the ferrous ion.

That this electronic structure description is reasonable is once again supported by the calculated Mössbauer parameters. In particular, the isomer shift of 0.45 mm/s is more than 0.2 mm/s larger than for the [Fe(gma)(X)] complexes and clearly indicates a different electronic situation in [Fe(PhBMA)]. This value is accurately reproduced by the calculations and indicates that the basic electronic structure description is correct. The computed quadrupole splitting is, unfortunately, significantly larger than the experimentally observed one, which is curiously small for a four-coordinated intermediate-spin Fe(II). Since the quadrupole splitting reacts much more sensitively to the complex geometry, there is the possibility that the calculated structure deviates significantly from reality. However, no experimental structure is available for [Fe(PhBMA)] to address this point in more detail.

To check whether the DFT methods we are using here have problems with intermediate spin Fe(II) complexes, we have carried out calculations on Sellmann's complex [Fe^{II}(C₆H₄S₂)₂]²⁻ (in these calculations additional diffuse functions were added to the basis set). This complex represents a clean intermediate-spin Fe(II) complex with essentially all of the spin located on the iron center. The computed Fe−S bond lengths of 2.271 Å and S−C bond lengths of 1.781 Å are in reasonable agreement with the experimental numbers[32,48] (Fe−S, 2.226 Å; S−C, 1.763 Å). Likewise, the computed isomer shift of 0.505 mm/s agrees well with the experimental value of 0.45 mm/s. However, the computed quadrupole splitting of 0.345 mm/s ($\eta = 0.207$) is significantly too small compared to 1.18 mm/s found experimentally. It thus appears that the field gradient in intermediate-spin Fe(II) complexes is not readily predicted correctly by DFT methods. A more detailed study of the origins for this failure appears to be necessary. However, based on the isomer shift results, we are confident that the assignment of intermediate-spin Fe(II) to [Fe(PhBMA)] is correct. It is conceivable that the isomer shift reacts less sensitively to the details of the electronic structure than the quadrupole splitting. In the presence of exceptionally strong spin−orbit coupling, as expected for intermediate-spin Fe(II), several multiplets may contribute to the electronic ground state. This effect is not included in our DFT calculations and a much more elaborate study could be necessary to clarify this point.

In conclusion, the calculations show that (PhBMA)²⁻ is an innocent ligand toward Fe(II) and the resulting complex is a genuine intermediate-spin Fe(II) species. The essential difference to the gma ligand is that PhBMA does *not* feature a low-lying LUMO orbital which could take up an electron from the central Fe(II).

c. Electronic Structure of [Fe(gma)(PR₃)₂]. A second interesting modification of the electronic structure pattern found for [Fe(gma)(X)] is the coordination of the sixth ligand as in

(48) Sellmann, D.; Geck, M.; Knoch, F.; Ritter, G.; Dengler, J. *J. Am. Chem. Soc.* **1991**, *113*, 3819.
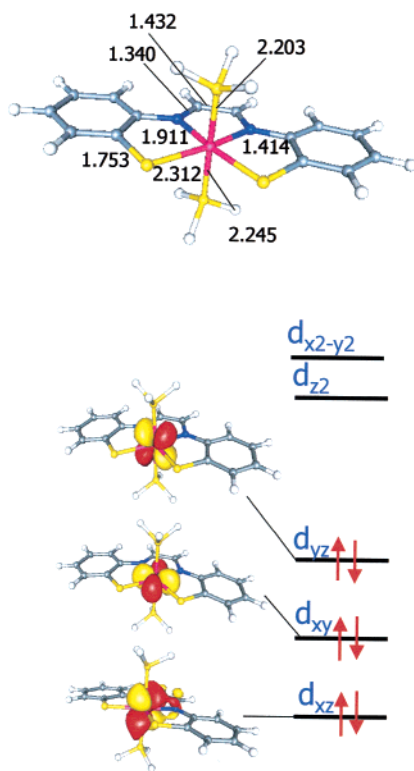
Figure 12. Calculated structure (top, distances in Å) and qualitative MO scheme (bottom) for [Fe(gma)(PH₃)₂]. The occupied orbitals are Pipek-Mezey localized orbitals from a spin unrestricted B3LYP calculation.

[Fe(gma)(PH₃)₂]. Again, this complex shows Mössbauer parameters which are clearly different and, in addition, features a $S = 0$ ground state. The calculated structure and the calculated bonding scheme for this complex are shown in Figure 12.

The interesting result is found, that in [Fe(gma)(PH₃)₂] electron transfer from Fe(II) to the gma ligand does *not* occur. Instead, the complex features a standard low-spin Fe(II) configuration with a $(t_{2g})^6$ electronic configuration. This is readily explained by ligand field theory. The sixth ligand greatly destabilizes the d_{z^2} orbital, which is consequently too high in energy to become occupied. This leaves the three iron based t_{2g} orbitals lower in energy and fully occupied, leading to a stable completely filled subshell. Back-bonding to π-accepting axial phosphines and, to a limited extent, to the low-lying LUMO of the gma ligand further lowers the energy of the t_{2g} set of orbitals and consequently they become too low in energy to promote an electron transfer into the LUMO of the diimine ligand. That this interpretation is correct is once more shown by the calculated Mössbauer parameters, which match the experimentally observed values reasonably well (the negative sign of the quadrupole splitting is of little relevance for an η of essentially unity). For comparison we have also carried out calculations for a BS solution, which corresponds to a low-spin Fe(III) (gma•)³⁻ situation. However, the energy of this solution is ~7 kcal/mol less stable than the closed-shell solution and in addition the calculated Mössbauer parameters $\delta_{MB} = 0.19$ mm/s and $\Delta E_Q = -2.15$ mm/s are in disagreement with the experimental findings.

In summary, the combination of theory with Mössbauer spectroscopy shows that the altered ligand field in [Fe(gma)-(PH₃)₂] prevents electron transfer to the gma ligand and results

in the closed-shell configuration $(d_{xy})^2(d_{xz})^2(d_{yz})^2(L(a_2))^2(L(b_2))^0$-$(d_{x^2-y^2})^0(d_{z^2})^0$.

d. Electronic Structure of [Fe(gma)(py)]⁺, [Fe(gma)(CN)], and [Fe(gma)I]. The most difficult electronic structure is found in the complexes [Fe(gma)(py)]⁺, [Fe(gma)(CN)], and [Fe-(gma)I], all of which have one valence electron less than the corresponding complexes [Fe(gma)(X)] (X = py, PH₃) discussed above. The puzzling observation is that these complexes show a spin state of $S = 1/2$. The most straightforward explanation of this result is that one electron has, in fact, been taken out of one of the iron-based MO's to produce an Fe(IV) electronic configuration with $S_{Fe} = 1$ and a ligand centered radical (gma•)³⁻. The valence-state Fe(IV) would have been clearly detected in the Mössbauer experiments. However, the Mössbauer experiments show that the local environment of the iron essentially does *not* change during oxidation. Thus, a change in the number of d-electrons or a change in spin state at the iron is excluded by the experimental results. Alternatively, if the electron is removed from the ligand, one would have anticipated that it is taken out of L(b₂), which would leave a closed-shell ligand and a total spin of $S = 3/2$. However, a total spin of $S = 1/2$ is clearly observed for [Fe(gma)(py)]⁺, [Fe-(gma)(CN)], and [Fe(gma)I]. This admittedly complicated problem finds its solution once more by DFT calculations, even if the calculations will turn out to be only partially successful for [Fe(gma)(CN)] and [Fe(gma)I].

The most striking observation is that the neutral cyano complex [Fe(gma)(CN)] shows essentially the same Mössbauer parameters as the reduced form, [Fe(gma)(CN)]⁻. We were unable to successfully reproduce this experimental finding for the cyano complexes (Table 6) which might be traced back to the observation that already [Fe(gma)(CN)]⁻ is not described well by the DFT calculations. We have therefore studied in detail the one-electron oxidized form of [Fe(gma)(py)], namely, its monocation, which *is* well described by the calculations. Several spin unrestricted DFT solutions have been obtained for [Fe-(gma)(py)]⁺, which correspond to the electronic structures Fe-(III)($S_{Fe} = 3/2$)/(gma)($S_{gma} = 0$), Fe(III)($S_{Fe} = 3/2$)/(gma)($S_{gma} = 1$), Fe(III)($S_{Fe} = 1/2$)/(gma)($S_{gma} = 0$), and Fe(IV)($S_{Fe} = 1$)/(gma•)($S_{gma} = 1/2$). Based on these calculations, the only plausible electronic structure which leaves the calculated Mössbauer parameters reasonably invariant between [Fe(gma)-(py)] and [Fe(gma)(py)]⁺ and which accounts for the observed spin states is Fe(III)($S_{Fe} = 3/2$)/(gma)($S_{gma} = 1$). For this formulation one observes a slight increase in the isomer shift upon oxidation but no significant change in the quadrupole splitting. *Thus, the one-electron oxidized forms correspond to the coupling of an intermediate spin Fe(III) to a ligand triplet state.* This interpretation is suggested by a combination of theory and experiment. It is also plausibly based on the observation that the first excited triplet state is low lying in [Zn(gma)] and [Ni(gma)]. *Still, the first triplet state of (gma)²⁻ is an excited state and therefore these complexes represent intriguing examples of what might be called "excited state" coordination chemistry.*

Based on the discussion given above, one expects *two* overlapping valence bond like pairs in the corresponding orbital analysis of the BS wave function. This expectation is confirmed and Figure 13 shows a qualitative bonding scheme for [Fe(gma)-(py)]⁺. The two "magnetic" pairs are formed between the metal
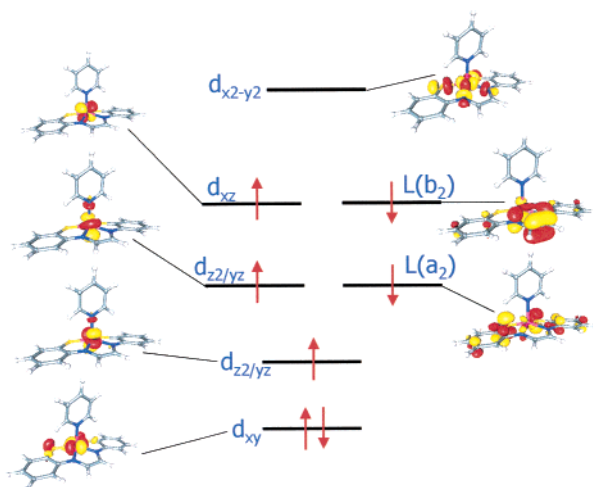
Figure 13. Qualitative bonding scheme for [Fe(gma)(py)] as derived from BS-B3LYP DFT calculations. The doubly occupied MO's are canonical MO's, and the singly occupied MO's result from a corresponding orbital transformation.

d_{xz} orbital and the ligand L(a$_2$) HOMO and second between the Fe d_{yz}-derived MO and the ligand L(b$_2$) LUMO. The d_{yz}/L(b$_2$) π-type interaction is fairly strong as indicated by a corresponding orbital overlap of 0.636 (note that there is some mixing between d_{yz} and d_{z^2} observed in Figure 13 which is of little consequences for the conclusions drawn here). The d_{xz}/L(a$_2$) interaction is weaker with an overlap of 0.447 and may also be viewed as a π-type interaction with the mainly sulfur-centered out-of-plane lone pairs that comprise the L(a$_2$) HOMO. The calculated exchange parameter of -842 cm^{-1} is fairly large and thermal population of any excited multiplet cannot be expected.

It is interesting to note that the first quartet state is calculated to be only 0.6 kcal/mol less stable than the $M_S = 1/2$ BS state at the B3LYP level. The quartet state corresponds to the intermediate spin Fe(III) configuration and the closed-shell gma ligand. As expected, the isomer shift obtained for the $S = 3/2$ state is similar to that for the $S = 1/2$ BS state. However, the quadrupole splitting increases significantly (Table 6), which is presumably due to the loss of a significant π-interaction between the Fe d_{yz} based MO and the ligand LUMO. Turning back to total energies a correction for the spin coupling between a $S = 3/2$ and a $S = 1$ species should be included in the energy difference which will work in favor of the $S = 1/2$ state. With a calculated J parameter of -843 cm^{-1}, the extra stabilization due to spin coupling amounts to as much as 4.8 kcal/mol. Thus, it may be hypothesized that the stabilization due to the strong spin coupling is an essential factor in favoring the $S = 1/2$ over the $S = 3/2$ state.

It is unfortunate that [Fe(gma)(py)]$^+$ could not be studied in detail experimentally. The situation is even more frustrating since we did not succeed in generating the corresponding BS solutions for [Fe(gma)(CN)] and [Fe(gma)I].

In the case of the cyano complex [Fe(gma)(CN)] the $M_S = 1/2$ BS converged to a solution that maybe described as Fe(III) ($S_{Fe} = 1/2$) coupled to a closed-shell ligand (gma)($S_{gma} = 0$). That this description is *not* appropriate is shown by the calculated Mössbauer parameters (Table 6). The calculated isomer shifts are far too small and the calculated quadrupole splittings are significantly too large. Moreover, from [Fe(gma)-(CN)]$^-$ to [Fe(gma)(CN)] a significant decrease in the isomer

shift and an increase in the quadrupole splitting is calculated, both results are in disagreement with experiment. We made numerous attempts to generate a correct electronic structure for [Fe(gma)(CN)] from various DFT methods which were, however, all without success. However, we feel that the electronic structure description offered for [Fe(gma)(py)]$^+$ also applies to [Fe(gma)(CN)]; namely, these complexes correspond to intermediate-spin Fe(III) sites coupled to the triplet state of the dianionic gma ligand. The obtained low-spin Fe(III) description may be interpreted as evidence for a too strong back-bonding interaction in the case of the CN$^-$ ligand which would stabilize the iron t$_{2g}$ like orbitals up to the point were a low-spin situation is energetically more favorable.

The situation is somewhat different for the iodide complex [Fe(gma)I]. Here we find a BS solution that may—in a limiting sense—be characterized as Fe(IV) ($S_{Fe} = 1$) coupled to a ligand trianionic radical gma$^{\bullet}$ ($S_{gma} = 1/2$). Again, the Mössbauer parameters are not in good agreement with the experimental values, and we have not studied this complex further due to our present inability to properly include relativistic effects in our DFT treatment. Most likely, the same electronic structure description that was found for [Fe(gma)(py)]$^+$ also applies to [Fe(gma)I] and the calculations tend to overestimate the stabilization of the Fe(IV) state by the soft iodide ligand which, in the calculations, shows an exceptionally strong charge donation to the iron, which amounts to almost 0.5 electrons.

Finally, the g-tensor of the systems studied in this paragraph will be discussed. In the strong exchange limit the g-tensor of the spin-coupled system can be written as[49]

$$\mathbf{g} = \frac{5}{3}(1g_e + \Delta\mathbf{g}_{Fe}) - \frac{2}{3}(1g_e + \Delta\mathbf{g}_{gma})$$

$$\approx 1g_e + \frac{5}{3}\Delta\mathbf{g}_{Fe} \qquad (3)$$

where we have assumed to a good approximation that $\mathbf{g}_{gma} = 1g_e$, where g_e is the free electron g-value and $\Delta\mathbf{g}_{Fe}$ and $\Delta\mathbf{g}_{gma}$ are the g-shifts due to the "intermediate-spin Fe(III) subsystem" and the "gma-triplet" subsystem, respectively. Thus, based on eq 3 the effect of the spin coupling is to enhance the g-shift of the intermediate spin iron by 67%. Since isolated intermediate-spin Fe(III) complexes have $S_t = 3/2$, their g-values are difficult to measure with high accuracy. In the study by Kostka et al. on the intermediate-spin Fe(III) complex [Fe(MAC*)Cl]$^{2-}$ (MAC* = 1,4,8,11-tetraaza-13,13-diethyl-2,2,5,5,7,7,10,10-octamethyl-3,6,9,12,14-pentaoxocyclotetradecane)[50] three positive g-shifts where found with $g_\perp = 2.03$ and $g_\parallel = 2.06$. In the present study g-values of 2.23, 2.13, and 2.01 where observed for [Fe(gma)I] and 2.23, 2.11, and 2.00 for [Fe(gma)(CN)] which show only a moderate dependence on the axial ligand. Thus, the spectra are consistent with enhanced g-values for an intermediate-spin Fe-(III). The origin of the g-shift can be interpreted from the electronic structure description given above and in Scheme 4. The SOC between the doubly occupied d_{xy} orbital and the singly occupied d_{xz} and d_{yz} orbitals will give positive contributions to the g-shifts along the x- and y-directions respectively, while there is no SOC between d_{xy} and the third singly occupied d_{z^2} orbital.

(49) Bencini, A.; Gatteschi, D. *EPR of Exchange Coupled Systems*; Springer: Heidelberg; 1990.
(50) Kostka, K. L.; Fox, B. G.; Hendrich, M. P.; Collins, T. J.; Rickard, C. E. F.; Wright, L. J.; Münck, E. *J. Am. Chem. Soc.* **1993**, *115*, 6746.

Scheme 4. Origin of *g*-Shifts in Intermediate-Spin Iron(III) Complexes
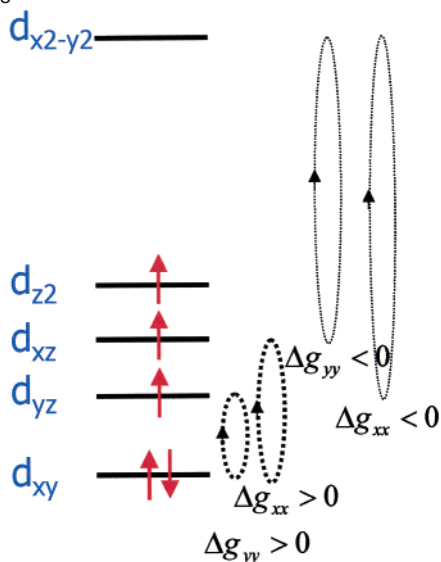
The SOC between the singly occupied d_{xz} and d_{yz} orbitals with the empty $d_{x^2-y^2}$ orbital contributes negative *g*-shifts along the *y*- and *x*-axes, respectively, while there is no contribution along the *z*-axis. Thus, depending on the relative positions of the singly occupied orbitals relative to the doubly occupied d_{xy} and the empty $d_{x^2-y^2}$ orbitals, one expects two *g*-shifts which are either positive or negative, while one *g*-value should remain close to 2. In the present case it is reasonable to assume that the $d_{x^2-y^2}$ orbital is too high in energy to give an appreciable contribution and consequently the positive *g*-shifts are mainly attributed to the SOC between the d_{xy} and the d_{xz} and d_{yz} orbitals.

In summary, the interaction between the metal and the ligand for the one-electron oxidized species [Fe(gma)(CN)], [Fe(gma)I], and [Fe(gma)(py)]$^+$ appears to be fairly complicated. Based on the experimental data and the calculations on [Fe(gma)(py)]$^+$, we favor a model in which an intermediate-spin Fe(III) ion (S_{Fe} = 3/2) is coordinated to an excited triplet state of the ligand (S_{gma} = 1) in all of these complexes to produce the electronic configuration $(d_{xy})^2(d_{xz})^1(d_{yz})^1(d_{z^2})^1(L(a_2))^1(L(b_2))^1(d_{x^2-y^2})^0$. Such a coordination mode is fairly unusual and more work is certainly needed to establish it unambiguously. In addition, for this particular case the DFT calculations have only met with partial success and we are currently extending our methodologies toward truly multiconfigurational ab initio methods that should provide a powerful arsenal of theoretical methods to study systems that are as complex as the molecules studied in this work.

Conclusions

In the present work we have discussed intriguing examples of metal−radical spin coupling on the basis of chemical synthesis, crystal structure determinations, spectroscopic measurements, and DFT calculations. The results conclusively show that the (gma)$^{2-}$ ligand has an exceptionally low lying LUMO orbital which readily accepts an electron to form (gma•)$^{3-}$. The occupation of the ligand LUMO either in its trianionic form or in the first excited triplet state (gma*)$^{2-}$ immediately leads to a significant shortening of the α-diimine C−C bond below 1.43 Å and a significant lengthening of the α-diimine C−N bond above 1.32 Å. This type of distortion has been most clearly

demonstrated by Gardiner et al.[39] who reported the crystal structure of [Li(1,4-di-*tert*-butyl-1,4-diazabutadiene)$_2$], which shows two very inequivalent ligands with C−C-bond lengths of 1.488 and 1.399 Å and C−N bond lengths of 1.236 and 1.317 Å, respectively. Thus, this system represents a mixed-valence situation with the extra electron being trapped on one of the ligands.

Due to the ease of reduction of the gma ligand, the complexes [Zn(gma•)]$^-$ and [Ni(gma•)]$^-$ are easily prepared electrochemically or chemically.[2] In these complexes the effective nuclear charge on the metal is too high to allow a full electron transfer from the metal to the ligand. However, as one moves down across the first transition row the d-orbital energies of the divalent ions increase and oxidation of the metal becomes more feasible. Thus Fe(II) is already electron donating enough to lead to a ground-state electronic structure description which features an intermediate-spin Fe(III) ion (S_{Fe} = 3/2) and a ligand radical (gma•)$^{3-}$ (S_{gma} = 1/2) to give a total spin of S_t = 1. This conclusion is in sharp contrast to previous investigations which assigned an intermediate-spin Fe(II) configuration to the various iron-gma complexes.[7] The only genuine intermediate-spin Fe-(II) complex in the series occurs with the ligand PhBMA which does *not* feature a low-lying LUMO and therefore acts as an innocent ligand toward Fe(II). Consequently, the spectroscopic properties of [Fe(PhBMA)] differ strongly from those of the iron-gma complexes. A second way to prevent electron transfer from the iron to the ligand is to coordinate a sixth strong π-acceptor ligand as in [Fe(gma)(PH$_3$)$_2$]. In this case the intermediate spin Fe(III) configuration becomes energetically unfavorable and a low-spin Fe(II) configuration with S_{Fe} = S_{gma} = S_t = 0 is adopted instead.

The most interesting case occurs in the species [Fe(gma)-(py)]$^+$, [Fe(gma)I], and [Fe(gma)(CN)], all of which possess a total spin of S_t = 1/2 and Mössbauer parameters that are essentially unchanged from their one-electron-reduced precursors. Our model for these complexes is that of an intermediate-spin Fe(III) ion with S_{Fe} = 3/2 which couples strongly antiferromagnetically to the first excited triplet state of the dianionic ligand, i.e., (gma*)$^{2-}$. The strong antiferromagnetic exchange coupling contributes as much as ~4.8 kcal/mol to the stabilization of the complex and is the main reason for favoring the excited triplet state of the ligand over the closed-shell ground state, which would result in a complex with S_t = 3/2.

We have labeled this apparently unprecedented coordination pattern as "excited state" coordination. However, some clarifications are necessary to distinguish it from other well-known phenomena in inorganic electronic structure.

First, the situation is different than for a paramagnetic central iron M coordinated to a ligand diradical (L•)$_2$ as described in detail in several papers on complexes of the form [M(L•)$_2$].[19,52] In this case it is sufficient that the nearest-neighbor antiferromagnetic exchange interaction dominates over the L−L antiferromagnetic coupling to give an apparent triplet coupling to the (L•)$_2$ unit. The present case is different because the orbitals involved in the triplet state of (gma*)$^{2-}$ are not "left" and "right" ligand-localized MO's or the symmetric and antisymmetric

(51) (a) Noodleman, L.; Baerends, E. J. *J. Am. Chem. Soc.* **1984**, *106*, 2316. (b) Le Pape, L.; Lamotte, B.; Mouesca, J. M.; Riu, G. *J. Am. Chem. Soc.* **1997**, *119*, 9757.
(52) Bachler, V.; Olbrich, G.; Neese, F.; Wieghardt, K. *Inorg. Chem.* **2002**, *41*, 4179.

combinations of two such MO's but are two spatially unrelated MO's. One is a π^*-orbital which is localized essentially on the α-diimine bridge, and the other one represents a lone pair on the coordinating sulfurs. Thus, in the first place it is the low-lying LUMO orbital of the α-diimine unit that leads to an accidental near-degeneracy of the ligand HOMO and LUMO and consequently to a low-lying first excited triplet state on the ligand.

Second, the situation found here is different than what has previously been called excited-state coordination chemistry.[53] These highly sophisticated investigations deal with coordination complexes in electronically excited states. The excitation changes, for example, the pK_a values of coordinating ligands and leads to marked changes in structural parameters. With sophisticated instrumentation these phenomena can be measured and analyzed in impressive detail.[53] However, in the present case we deal with complexes in their electronic ground states and claim that one of the coordinating fragments is in an internally excited state, which is different from the situation found in short lived electronically excited states. What we describe is an interpretation of a peculiar bonding situation. In a strict physical sense it does not represent an observable property, since observables always refer to the whole system and not to its parts. It is, however, a description of the bonding in a chemically appealing language which is suggested by both the experimental results as well as the results of electronic structure calculations, and we feel that it is a chemically meaningful model.

It is stressed that it is the combination of experiment and theory which has led to considerable insight into the electronic structures and bonding properties of the molecules studied in this work. The electronic structure calculations are of great utility not only in predicting or reproducing experimentally determined numbers but in providing intuitively appealing pictures of the bonding in the molecules under investigation and therefore inspire new experiments. On the other hand, the calculations can occasionally fail to provide physically sensible results. We believe that it is important to detect these situations in order to avoid misinterpretations. The sensitivity of the optical and magnetic properties of coordination complexes to their electronic structures provides a powerful link between theory and experiment. However, to use this link to its full potential requires the ability to predict properties such as EPR *g*-values, hyperfine couplings, or Mössbauer parameters at the same level of theory that is used to arrive at qualitative interpretations or quantitative energetic predictions. We therefore feel that the development of such methods[9−16] constitutes an important progress in inorganic electronic structure research that is being made in recent years.

Supporting Information Available: Details of X-ray crystallographic data collection and structure refinement and tables of atomic coordinates, bond distances and angles, anisotropic thermal parameters, and hydrogen atom positions for **6**. This material is available free of charge via the Internet at http://pubs.acs.org.

JA021123H

(53) For recent reviews, see: (a) Coppens, P.; Novozhilova, I.; Kovalevsky, A. *Chem. Rev.* **2002**, *102*, 861. (b) Kim, C. D.; Pillet, S.; Wu, G.; Fullgar, W. K.; Coppens, P. *Acta Crystallogr. A* **2002**, *58*, 133. (c) Hicks, C.; Ye, G. Z.; Levi, C.; Gonzales, M.; Rutenburg, I.; Fan, J. W.; Helmy, R.; Kassis, A.; Gafney, H. D. *Coord. Chem. Rev.* **2001**, *211*, 207.